Corrected 20 April 2008

MULTIPLE SCATTERING, RADIATIVE TRANSFER, AND WEAK LOCALIZATION IN DISCRETE RANDOM MEDIA: UNIFIED MICROPHYSICAL APPROACH

Michael I. Mishchenko[1]

Received 13 June 2007; accepted 25 September 2007; published 19 April 2008.

[1] The radiative transfer theory has been extensively used in geophysics, remote sensing, and astrophysics for more than a century, but its physical basis had remained uncertain until quite recently. This ambiguous situation has finally changed, and the theory of radiative transfer in random particulate media has become a legitimate branch of Maxwell's electromagnetics. This tutorial review is intended to provide an accessible outline of recent basic developments. It discusses elastic electromagnetic scattering by random many-particle groups and summarizes the unified microphysical approach to radiative transfer and the effect of weak localization of electromagnetic waves (otherwise known as coherent backscattering). It explains the exact meaning of such fundamental concepts as single and multiple scattering, demonstrates how the theories of radiative transfer and weak localization originate in the Maxwell equations, and exposes and corrects certain misconceptions of the traditional phenomenological approach to radiative transfer. It also discusses the challenges facing the theories of multiple scattering, radiative transfer, and weak localization in the context of geophysical applications.

Citation: Mishchenko, M. I. (2008), Multiple scattering, radiative transfer, and weak localization in discrete random media: Unified microphysical approach, *Rev. Geophys.*, *46*, RG2003, doi:10.1029/2007RG000230.

1. INTRODUCTION

[2] The early history of the phenomenological theory of radiative transfer (RT) describing electromagnetic energy transport in macroscopic media composed of sparsely and randomly distributed, elastically scattering particles is described by *Ivanov* [1994]. He traces the origin of the simplest form of the RT equation (RTE), no account of polarization, idealized isotropically scattering particles, to papers by *Lommel* [1887] and *Chwolson* [1889]. Unfortunately, these early publications have been hardly noticed, and the first introduction of the RTE has traditionally been attributed to the paper by *Schuster* [1905].

[3] *Gans* [1924] was the first to account for the polarization nature of light in the context of the phenomenological RT theory. However, he analyzed only the special case of a plane-parallel Rayleigh-scattering medium illuminated by perpendicularly incident light and considered only the first two components of the Stokes column vector. The case of arbitrary illumination and arbitrary polarization was first studied by *Chandrasekhar* [1950], but his analysis was again limited to Rayleigh-scattering particulate media [see also *Chandrasekhar*, 1989]. Finally, *Rozenberg* [1955] introduced the most general form of the RTE, the so-called vector RTE, which fully accounts for the polarization nature of light and is applicable to scattering media composed of arbitrarily shaped and arbitrarily oriented particles.

[4] Since its inception, the RT theory has had a remarkable history of practical applications in numerous areas of atmospheric radiation [*Hansen and Travis*, 1974; *Sobolev*, 1975; *van de Hulst*, 1980; *Lenoble*, 1985, 1993; *Goody and Yung*, 1989; *Liou*, 1992, 2002; *Yanovitskij*, 1997; *Marshak and Davis*, 2005; *Bohren and Clothiaux*, 2006; *Zdunkowski et al.*, 2007], remote sensing [*Ishimaru*, 1978; *Ulaby and Elachi*, 1990; *Fung*, 1994; *Stephens*, 1994], oceanography [*Mobley*, 1994; *Thomas and Stamnes*, 1999], image transfer [*Zege et al.*, 1991], astrophysics [*Hansen and Hovenier*, 1974; *Dolginov et al.*, 1995], biomedicine [*Khlebtsov et al.*, 2002; *Tuchin et al.*, 2006], and engineering [*Viskanta and Mengüç*, 1987; *Siegel and Howell*, 2002; *Modest*, 2003]. At the same time, it has also had a long history of confusing and even misleading accounts of its fundamental principles. The palette of phenomenological derivations of the RTE encountered in various monographs, textbooks, and reviews is quite rich, which by itself is a sign of a serious problem. On one hand, most of the derivations are rather short and either present the RTE as a trivial consequence of energy conservation or expect the reader to accept the RTE as a fundamental experimental law implicitly supplementing other basic physical principles such as the laws of classical

[1]NASA Goddard Institute for Space Studies, New York, New York, USA.

and quantum electrodynamics. On the other hand, there are derivations that rise to the level of a philosophical essay in which the RTE emerges as an allegedly logical outcome of a multipage discourse almost devoid of formulas but full of ill-defined collective effects, elementary volume elements, and incoherent light rays. Some of the derivations even invoke the concept of photons as localized particles of light, discrete blobs of energy without phases, or corpuscles that are moving according to the laws of classical mechanics. As such, they imply that the notorious wave-particle duality of light somehow manifests itself in the scattering process that is fully controlled by the Maxwell equations.

[5] The "photonic" language [*Pomraning*, 1973; *Mihalas and Weibel-Mihalas*, 1984; *Oxenius*, 1986] can be especially inaccurate and misleading when applied to elastically scattering, macroscopic particulate media. Indeed, one is expected to accept that light propagates as a stream of photons between the particles, decides to become a wave when it impinges upon a particle and thereby generates a multitude of spectacular effects such as diffraction, glory, morphology-dependent resonances, etc. [*Mishchenko et al.*, 2002], and then changes its mind again upon leaving the particle and resumes its journey in the form of photons. The physical insolvency of this juggling with waves and photons is obvious. First of all, it is the process of interaction of light with matter that may require quantization of energy not the process of light propagation. Second, photons appear as the result of quantization of the electromagnetic field. Therefore, whatever is called a "photon" in order to derive the RTE remains an imaginary object with no physical meaning unless the electromagnetic field is quantized explicitly. Needless to say, the latter is never done. Third, it takes opening a standard textbook on quantum electrodynamics or quantum optics [*Power*, 1964; *Akhiezer and Berestetskii*, 1965; *Mandel and Wolf*, 1995; *Meystre and Sargent*, 1999] to realize that a photon is a quantum of a single normal mode of the electromagnetic field and as such is associated with a plane wave of definite wave vector but infinite lateral extent. Therefore, photons are not localized particles of light [*Kidd et al.*, 1989; *Lamb*, 1995] and cannot be used to define quantities such as the specific intensity or the specific intensity column vector [*Wolf*, 1978]. Fourth, it is well established, albeit not widely publicized, that the alleged particle behavior of light in phenomena such as the photoelectric and Compton effects is explainable in terms of the semiclassical approach wherein the electromagnetic field is not quantized and is described by the classical Maxwell equations [*Schiff*, 1968; *Kidd et al.*, 1989; *Fearn and Lamb*, 1991; *Lamb*, 1995].

[6] One of the pioneers of lasers and misers Charles H. Townes remarked [*Townes*, 1984, p. 547] that "physicists were somewhat diverted by an emphasis in the world of physics on the photon properties of light rather than its coherent aspects." This remark remains quite topical.

[7] No matter how realistic the various phenomenological accounts of RT may look at first sight [*Preisendorfer*, 1965], they inevitably fall apart upon scrutiny of their physical foundation [*Apresyan and Kravtsov*, 1996]. It is therefore not surprising that quite recently, *Mandel and Wolf* [1995, p. 302] stated that "in spite of the extensive use of the theory of radiative energy transfer, no satisfactory derivation of its basic equation from electromagnetic theory has been obtained up to now." Furthermore, the phenomenological accounts completely overlook the fundamental link between RT and the effect of weak localization (WL) of electromagnetic waves in the backscattering direction (otherwise known as the effect of coherent backscattering). Most importantly, they conceal the irrefutable fact that as long as scattering occurs without frequency redistribution and the particles are macroscopic and can be characterized by a refractive index, the RTE describes multiple scattering of classical electromagnetic waves and, as such, must be derived directly from the macroscopic Maxwell equations via a series of well-defined and reproducible analytical steps [*Borovoy*, 1966; *Barabanenkov*, 1975; *Tsang et al.*, 1985].

[8] This ambiguous situation has finally changed, and a complete derivation of the vector RTE directly from the macroscopic Maxwell equations for the case of elastically scattering discrete random media has been published [*Mishchenko*, 2002, 2003; *Mishchenko et al.*, 2006a]. This derivation can be used to clarify the role and physical meaning of the various quantities entering the RTE, establish a direct link between the theories of RT and WL, cross-examine the terminologies used in the traditional phenomenological and the new microphysical approaches, and identify and correct certain misconceptions of the phenomenological approach. These are the four principal goals of this tutorial review. The overall objective is not to replace recent monographs such as those by *Tsang and Kong* [2001], *Hovenier et al.* [2004], *Martin* [2006], and *Mishchenko et al.* [2006a] but rather to provide a brief yet coherent outline that could convince the reader that the microphysical approach to RT and WL is both necessary, feasible, and fruitful. The challenges facing the theories of multiple scattering, RT, and WL in the context of geophysical applications are also classified and analyzed. Since the emphasis is on the fundamentals of the multiple scattering, RT, and WL theories, specific analytical and numerical techniques for solving the RTE (such as the adding-doubling, discrete ordinate, and Monte Carlo methods) and practical applications are not discussed.

2. BASIC ASSUMPTIONS

[9] Terrestrial clouds consisting of randomly positioned and randomly moving water droplets or ice crystals are typical examples of so-called discrete (or particulate) random media. The phenomenological theory of RT treats a cloud as a fictitious continuous medium in which the primary building unit is a vaguely defined elementary (or differential) volume element. In contrast, the microphysical theories of RT and WL account for the actual existence of particles as discrete inclusions with a refractive index different from that of the surrounding medium. Another fundamental difference is that the microphysical approach explicitly starts with the Maxwell equations as basic phys-

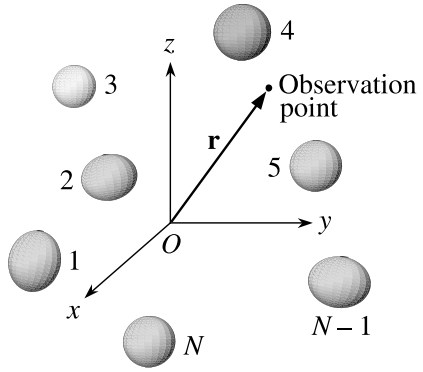

Figure 1. Scattering object in the form of a group of N discrete particles.

ical laws governing the process of interaction of electromagnetic radiation with matter and invokes no ad hoc physical concepts and laws not already contained in classical electromagnetics. The word "microphysical" then serves to emphasize the direct traceability of the RT and WL theories from fundamental physics not afforded by the phenomenological approach.

[10] Specifically, the microphysical theories of RT and WL rest on the following well-defined assumptions intended to formulate the overall problem in strict physical terms:

[11] 1. At each moment in time, the entire scattering object (e.g., a cloud of water droplets or a powder surface) can be represented by a specific spatial configuration of a number N of discrete finite particles (Figure 1). The unbounded host medium surrounding the scattering object is homogeneous, linear, isotropic, and nonabsorbing. Each particle is sufficiently large so that its atomic structure can be ignored and the particle can be characterized by optical constants appropriate to bulk matter. In electromagnetic terms, the presence of a particle means that the optical constants inside the particle volume are different from those of the surrounding host medium.

[12] 2. The entire scattering object is illuminated by either (1) a plane electromagnetic wave given by

$$\left.\begin{aligned}\mathbf{E}^{\rm inc}(\mathbf{r},t)&=\mathbf{E}_0^{\rm inc}\exp\left(\mathrm{i}\mathbf{k}^{\rm inc}\cdot\mathbf{r}-\mathrm{i}\omega t\right)\\ \mathbf{H}^{\rm inc}(\mathbf{r},t)&=\mathbf{H}_0^{\rm inc}\exp\left(\mathrm{i}\mathbf{k}^{\rm inc}\cdot\mathbf{r}-\mathrm{i}\omega t\right)\end{aligned}\right\}\quad \mathbf{r}\in\Re^3 \tag{1}$$

with constant amplitudes $\mathbf{E}_0^{\rm inc}$ and $\mathbf{H}_0^{\rm inc}$, where $\mathbf{E}$ is the electric field and $\mathbf{H}$ the magnetic field, t is time, $\mathbf{r}$ is the position (radius) vector, ω is the angular frequency, $\mathbf{k}^{\rm inc}$ is the real-valued wave vector, $\mathrm{i}=(-1)^{1/2}$, and $\Re^3$ denotes the entire three-dimensional space; or (2) a quasi-monochromatic parallel beam of light given by

$$\left.\begin{aligned}\mathbf{E}^{\rm inc}(\mathbf{r},t)&=\mathbf{E}_0^{\rm inc}(t)\exp\left(\mathrm{i}\mathbf{k}^{\rm inc}\cdot\mathbf{r}-\mathrm{i}\omega t\right)\\ \mathbf{H}^{\rm inc}(\mathbf{r},t)&=\mathbf{H}_0^{\rm inc}(t)\exp\left(\mathrm{i}\mathbf{k}^{\rm inc}\cdot\mathbf{r}-\mathrm{i}\omega t\right)\end{aligned}\right\}\quad \mathbf{r}\in\Re^3, \tag{2}$$

where fluctuations in time of the complex amplitudes of the electric and magnetic fields, $\mathbf{E}_0^{\rm inc}(t)$ and $\mathbf{H}_0^{\rm inc}(t)$, around their respective mean values occur much more slowly than the harmonic oscillations of the time factor $\exp(-\mathrm{i}\omega t)$. This restriction explicitly excludes other types of illumination such as a focused laser beam of finite lateral extent or a pulsed beam.

[13] 3. Nonlinear optics effects are excluded by assuming that the optical constants of both the scattering object and the surrounding medium are independent of the electric and magnetic fields.

[14] 4. It is assumed that electromagnetic scattering is elastic. This means that scattering occurs without frequency redistribution, that is, the scattered light has the same frequency as the incident light. This restriction excludes inelastic scattering phenomena such as Raman and Brillouin scattering as well as the specific consideration of the small Doppler shift of frequency of the scattered light relative to that of the incident light due the movement of the particles with respect to the source of illumination.

[15] 5. It is assumed that any significant changes in the scattering object (e.g., changes in particle positions and/or orientations with respect to the laboratory reference frame) occur over time intervals T much longer than the period of time-harmonic oscillations of the electromagnetic field: $T\gg 2\pi/\omega$.

[16] 6. The phenomenon of thermal emission is excluded. This assumption is usually valid for objects at room or lower temperature and for short-wave infrared and shorter wavelengths.

3. MACROSCOPIC MAXWELL EQUATIONS

[17] The assumptions listed in section 2 imply that all fields and sources are time-harmonic and allow one to fully describe the total electromagnetic field at any moment in time everywhere in space as the solution of the so-called frequency domain macroscopic differential Maxwell equations [*Stratton*, 1941; *Jackson*, 1999; *Rothwell and Cloud*, 2001; *Van Bladel*, 2007]. The specific dependence of the optical constants on spatial coordinates and the corresponding boundary conditions at any moment are fully defined by the instantaneous geometrical configuration of the N particles (Figure 1).

[18] Specifically, it is convenient to factor out the time-harmonic dependence of the electric and magnetic fields: $\mathbf{E}(\mathbf{r},t)=\exp(-\mathrm{i}\omega t)\mathbf{E}(\mathbf{r})$ and $\mathbf{H}(\mathbf{r},t)=\exp(-\mathrm{i}\omega t)\mathbf{H}(\mathbf{r})$. The frequency domain monochromatic Maxwell curl equations describing the scattering problem in terms of the electric and magnetic field amplitudes $\mathbf{E}(\mathbf{r})$ and $\mathbf{H}(\mathbf{r})$ can then be written as follows:

$$\left.\begin{aligned}\nabla\times\mathbf{E}(\mathbf{r})&=\mathrm{i}\omega\mu_0\mathbf{H}(\mathbf{r})\\ \nabla\times\mathbf{H}(\mathbf{r})&=-\mathrm{i}\omega\epsilon_1\mathbf{E}(\mathbf{r})\end{aligned}\right\}\quad \mathbf{r}\in V_{\rm EXT}, \tag{3}$$

$$\left.\begin{aligned}\nabla\times\mathbf{E}(\mathbf{r})&=\mathrm{i}\omega\mu_0\mathbf{H}(\mathbf{r})\\ \nabla\times\mathbf{H}(\mathbf{r})&=-\mathrm{i}\omega\epsilon_2(\mathbf{r},\omega)\mathbf{E}(\mathbf{r})\end{aligned}\right\}\quad \mathbf{r}\in V_{\rm INT}. \tag{4}$$

In these equations, $V_{\rm INT}$ is the cumulative "interior" volume occupied by the scattering object; $V_{\rm EXT}$ is the infinite exterior region such that $V_{\rm INT}\cup V_{\rm EXT}=\Re^3$; the host medium and the scattering object are assumed to be nonmagnetic; μ_0 is the permeability of a vacuum; ϵ_1 is the real-

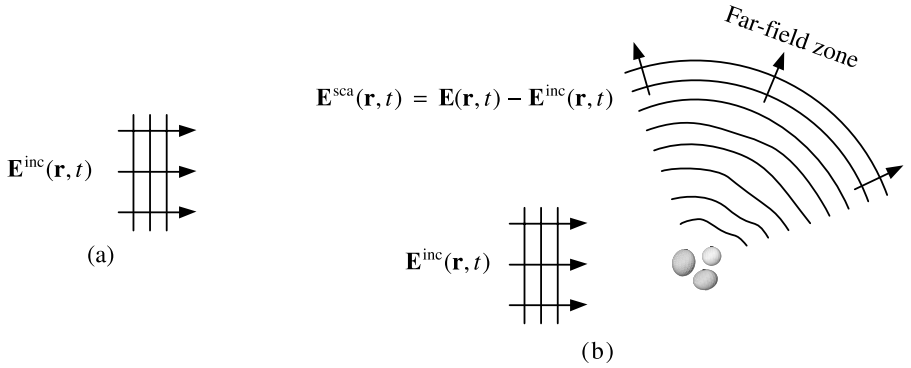

Figure 2. Scattering by a fixed finite object. (a) Total electric field in the absence of the scattering object. (b) Total electric field in the presence of the object decomposed into the incident and scattered fields. In this case the object consists of three disjoint, stationary particles.

valued electric permittivity of the host medium; and $\epsilon_2(\mathbf{r}, \omega)$ is the complex permittivity of the scattering object. Since the first relations in equations (3) and (4) yield the magnetic field provided that the electric field is known everywhere, the solution of equations (3) and (4) is usually sought in terms of only the electric field.

[19] Although the amplitudes $\mathbf{E}(\mathbf{r})$ and $\mathbf{H}(\mathbf{r})$ do not depend on time explicitly, they can change in time implicitly if the incident light is quasi-monochromatic and/or as a consequence of temporal variability of the scattering object. However, such changes occur much more slowly than the time-harmonic oscillations described by the factor $\exp(-i\omega t)$, which justifies the use of the frequency domain Maxwell equations.

[20] It should be recognized that macroscopic electromagnetics ignores the discreteness of matter forming the scattering particles and operates with continuous sources of fields. Therefore, its predictions can fall short in cases where quantum effects are important. Even so, the quantum theory can often be used to determine the macroscopic electromagnetic properties of bodies consisting of very large numbers of atoms [*Akhiezer and Peletminskii*, 1981]. This approach works for particles larger than about 50 Å [*Huffman*, 1988], thereby implying a very wide range of validity of macroscopic electromagnetics. Thus, our use of macroscopic electromagnetics as the point of departure is founded on the well-established fact that this theory follows directly from more fundamental physical theories as a consequence of well-characterized and verifiable approximations. In other words, the equations of classical macroscopic electromagnetics are accepted here essentially as basic axioms valid in a wide and well-defined range of relevant situations. The reader will see that this approach allows the development of a self-contained and self-consistent theory in which the need to invoke alternative physical concepts and laws is completely obviated.

4. ELECTROMAGNETIC SCATTERING

[21] The term "electromagnetic scattering" has been used until now without a prior strict definition. We will now fill this gap.

[22] The fundamental solution of the Maxwell equations in the form of a time-harmonic plane electromagnetic wave (equation (1)) represents the transport of electromagnetic energy from one point to another and embodies the concept of a perfectly monochromatic parallel beam of light. A plane electromagnetic wave propagates in an infinite nonabsorbing medium without a change in its intensity or polarization state (see Figure 2a). However, the presence of a finite object modifies the electromagnetic field that would otherwise exist in the unbounded homogeneous space. This modification is called electromagnetic scattering.

[23] The difference between the total field in the presence of the object, $\mathbf{E}(\mathbf{r}, t)$, and the original field that would exist in the absence of the object, $\mathbf{E}^{\rm inc}(\mathbf{r}, t)$, can be thought of as the field scattered by the object, $\mathbf{E}^{\rm sca}(\mathbf{r}, t)$ (Figure 2b). In other words, the total field in the presence of the object is represented as the vector sum of the respective incident (original) and scattered fields:

$$\mathbf{E}(\mathbf{r},t) = \mathbf{E}^{\rm inc}(\mathbf{r},t) + \mathbf{E}^{\rm sca}(\mathbf{r},t). \tag{5}$$

[24] The reader should recognize that the separation of the total field into the incident and scattered fields according to equation (5) is a purely mathematical procedure. This means that classical frequency domain electromagnetic scattering is not a physical process per se but rather an abbreviated way to state that the total field computed in the presence of an object is different from that computed in the absence of the object. To "describe electromagnetic scattering" then means to quantify the difference between the two fields as a function of the object's physical properties.

[25] To appreciate this fundamental point, let us recall that a plane electromagnetic wave is a stationary solution of the Maxwell equations in that it is assumed to have existed forever and, apart from the time-harmonic factor $\exp(-i\omega t)$, with no temporal change. The solution of the frequency domain Maxwell equations in the presence of the scattering object is also stationary. This implies that the scattered field is also stationary since it is defined mathematically as the difference between two stationary fields. Therefore, scattering of a time-harmonic electromagnetic wave is not a

temporally discrete event and cannot be visualized, for example, in terms of a light ray (or a localized blob of energy) approaching the object, then being scattered, and then propagating in an outward direction.

[26] We have already mentioned that the practical applicability of the frequency domain formalism implies the stationarity of the electromagnetic field over a time interval long compared with the period of time-harmonic oscillations. Therefore, this formalism can be used to describe scattering of quasi-monochromatic as well as monochromatic light.

[27] An especially transparent description of electromagnetic scattering is afforded by the so-called volume integral equation (VIE) that follows from the frequency domain macroscopic Maxwell equations and is exact [*Saxon*, 1955; *Mishchenko et al.*, 2002]:

$$\begin{aligned}\mathbf{E}(\mathbf{r}) &= \mathbf{E}^{\rm inc}(\mathbf{r}) + k_1^2 \int_{V_{\rm INT}} d\mathbf{r}' \overleftrightarrow{G}(\mathbf{r},\mathbf{r}') \cdot \mathbf{E}(\mathbf{r}') \left[m^2(\mathbf{r}') - 1\right] \\ &= \mathbf{E}^{\rm inc}(\mathbf{r}) + k_1^2 \left(\overleftrightarrow{I} + \frac{1}{k_1^2} \nabla \otimes \nabla\right) \\ &\quad \cdot \int_{V_{\rm INT}} d\mathbf{r}' \mathbf{E}(\mathbf{r}') \frac{\exp(ik_1|\mathbf{r}-\mathbf{r}'|)}{4\pi|\mathbf{r}-\mathbf{r}'|} \left[m^2(\mathbf{r}') - 1\right], \quad \mathbf{r} \in \Re^3, \end{aligned} \tag{6}$$

where the common factor $\exp(-i\omega t)$ is omitted, $m(\mathbf{r}') = [\epsilon_2(\mathbf{r}', \omega)/\epsilon_1]^{1/2}$ is the refractive index of the interior relative to that of the host exterior medium, $k_1 = |\mathbf{k}^{\rm inc}| = \omega(\epsilon_1\mu_0)^{1/2}$ is the wave number in the host medium, $\overleftrightarrow{G}(\mathbf{r}, \mathbf{r}')$ is the free space dyadic Green's function, $\overleftrightarrow{I}$ is the identity dyadic, and $\otimes$ is the dyadic product sign (see Appendix A for a brief overview of dyads and dyadics). One can see that the VIE expresses the total field everywhere in space in terms of the total internal field. If the scattering object is absent, $m(\mathbf{r}') \equiv 1$, then the total field is identically equal to the incident field. Otherwise, the total field contains a scattering component given by the second term on the right-hand side of equation (6). Since the internal field is not known in general, it must be found by solving the VIE either analytically or numerically.

[28] The VIE makes explicit two fundamental facts. First, the phenomenon of electromagnetic scattering is not limited to the case of the incident field in the form of a plane electromagnetic wave. In fact, it encompasses any incident field as long as the latter satisfies the Maxwell equations, e.g., spherical and cylindrical electromagnetic waves.

[29] Second, irrespective of the morphological structure of the scattering object, the latter remains a single, unified scatterer. Although the human eye may classify the scattering object as a "collection of discrete particles," the incident field always perceives the object as one scatterer in the form of a specific spatial distribution of the relative refractive index. The latter point can be made even more explicit by expressing the scattered electric field in terms of the incident field:

$$\mathbf{E}^{\rm sca}(\mathbf{r}) = \int_{V_{\rm INT}} d\mathbf{r}' \overleftrightarrow{G}(\mathbf{r},\mathbf{r}') \cdot \int_{V_{\rm INT}} d\mathbf{r}'' \overleftrightarrow{T}(\mathbf{r}',\mathbf{r}'') \cdot \mathbf{E}^{\rm inc}(\mathbf{r}''), \quad \mathbf{r} \in \Re^3, \tag{7}$$

where $\overleftrightarrow{T}$ is the so-called dyadic transition operator of the scattering object [*Tsang et al.*, 1985].

[30] Substituting equation (7) in equation (6) yields the following integral equation for $\overleftrightarrow{T}$:

$$\begin{aligned}\overleftrightarrow{T}(\mathbf{r},\mathbf{r}') &= k_1^2 \left[m^2(\mathbf{r}) - 1\right] \delta(\mathbf{r}-\mathbf{r}') \overleftrightarrow{I} \\ &\quad + k_1^2 \left[m^2(\mathbf{r}) - 1\right] \int_{V_{\rm INT}} d\mathbf{r}'' \overleftrightarrow{G}(\mathbf{r},\mathbf{r}'') \\ &\quad \cdot \overleftrightarrow{T}(\mathbf{r}'',\mathbf{r}'), \qquad \mathbf{r},\mathbf{r}' \in V_{\rm INT}, \end{aligned} \tag{8}$$

where $\delta(\mathbf{r})$ is the three-dimensional delta function. Equations of this type appear in the quantum theory of scattering and are called Lippmann-Schwinger equations [*Newton*, 1982]. The advantage of equations (7) and (8) is that $\overleftrightarrow{T}$ is the property of the scattering object only and is independent of the incident field. Furthermore, $\overleftrightarrow{T}$ provides a complete description of electromagnetic scattering by the object for any incident time-harmonic field. We will see in section 8 that the concept of dyadic transition operator plays a central role in the theory of multiple scattering.

[31] The ubiquitous presence of electromagnetic scattering in natural and artificial environments explains its fundamental importance in accurate modeling of electromagnetic energy transport for various science and engineering applications. This is also true of the situations in which electromagnetic scattering is induced artificially and used for particle characterization purposes. The exact theoretical and numerical techniques for the computation of the electromagnetic field elastically scattered by a finite fixed object composed of one or several particles are many and are reviewed thoroughly by *Mishchenko et al.* [2000, 2002], *Kahnert* [2003], *Babenko et al.* [2003], and *Doicu et al.* [2006]. All of these techniques have certain practical limitations in terms of the object morphology and object size relative to the incident wavelength and cannot be used yet to describe electromagnetic scattering by large multiparticle objects such as atmospheric clouds, particulate surfaces, and particle suspensions. This makes imperative the use of well-characterized approximate solutions that do not require unrealistic computer resources while being sufficiently accurate for specific applications. One of the main objectives of this review is to demonstrate that the microphysical theories of RT and WL are two such approximations.

[32] While the scattering of a time-harmonic electromagnetic wave is not a temporally discrete event, one can also consider the scattering of ultrashort electromagnetic pulses and thereby explicitly trace the temporal evolution of the electromagnetic field in space. This exercise provides a more intuitive visualization of scattering as a temporal event (D. Mackowski, personal communication, 2007) but, in general, requires one to solve explicitly the original time domain Maxwell equations. Doing this is possible in principle [*Taflove and Hagness*, 2000] but limits considerably the range of problems that can be solved analytically and numerically. This explains our preference to stay in the realm of the frequency domain electromagnetics.

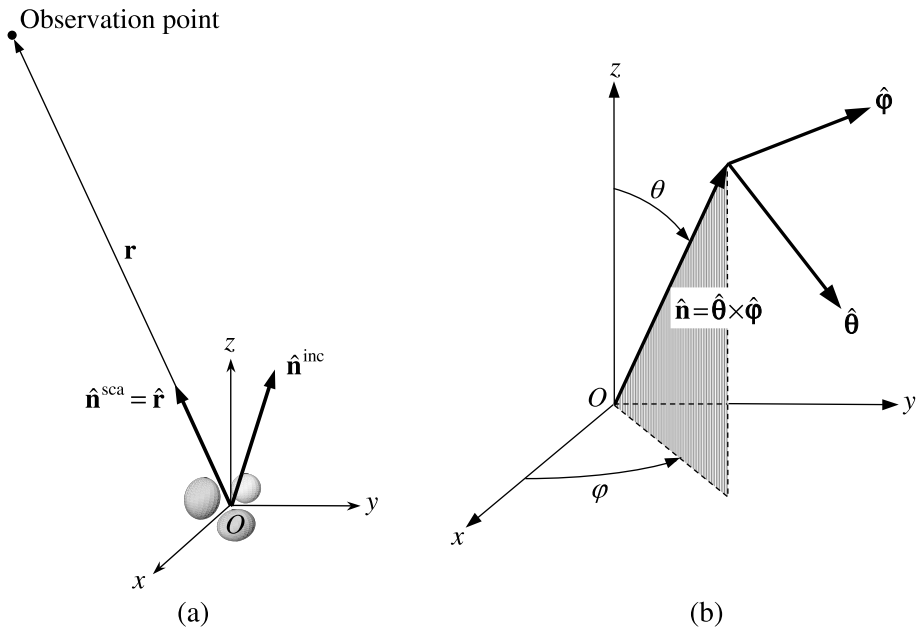

Figure 3. (a) Scattering in the far-field zone of the entire object. (b) Right-handed spherical coordinate system.

[33] Oliver Heaviside (1850–1925) was apparently the first to introduce the general concept of electromagnetic scattering in the context of Maxwell's theory [*Heaviside*, 1950]. Formal mathematical aspects of the electromagnetic scattering theory, including basic existence and uniqueness theorems, are discussed by *Müller* [1957], *Colton and Kress* [1998], *Doicu et al.* [2000], and *Pike and Sabatier* [2001].

5. FAR-FIELD AND NEAR-FIELD SCATTERING

[34] A fundamental property of the dyadic Green's function is the following asymptotic behavior:

$$\overleftrightarrow{G}(\mathbf{r},\mathbf{r}') \underset{r\to\infty}{\to} \left(\overleftrightarrow{I}-\hat{\mathbf{r}}\otimes\hat{\mathbf{r}}\right)\frac{\exp(ik_1 r)}{4\pi r}\exp(-ik_1\hat{\mathbf{r}}\cdot\mathbf{r}'), \qquad (9)$$

where $r = |\mathbf{r}|$ and $\hat{\mathbf{r}} = \mathbf{r}/r$. Placing the origin of the laboratory coordinate system O close to the geometrical center of the scattering object (Figure 3a) and substituting equations (1) and (9) in equation (7) yields [*Mishchenko et al.*, 2002, 2006a]

$$\mathbf{E}^{\rm sca}(\mathbf{r}) \underset{r\to\infty}{\to} \frac{\exp(ik_1 r)}{r}\mathbf{E}_1^{\rm sca}(\hat{\mathbf{n}}^{\rm sca}) = \frac{\exp(ik_1 r)}{r}\overleftrightarrow{A}(\hat{\mathbf{n}}^{\rm sca},\hat{\mathbf{n}}^{\rm inc}) \cdot \mathbf{E}_0^{\rm inc}, \qquad \hat{\mathbf{n}}^{\rm sca}\cdot\mathbf{E}_1^{\rm sca}(\hat{\mathbf{n}}^{\rm sca}) = 0, \qquad (10)$$

where $\hat{\mathbf{n}}^{\rm inc} = \mathbf{k}^{\rm inc}/k_1$ is a unit vector in the incidence direction; $\hat{\mathbf{n}}^{\rm sca} = \hat{\mathbf{r}}$ is a unit vector in the scattering direction; and $\overleftrightarrow{A}$ is the so-called scattering dyadic such that

$$\hat{\mathbf{n}}^{\rm sca}\cdot\overleftrightarrow{A}(\hat{\mathbf{n}}^{\rm sca},\hat{\mathbf{n}}^{\rm inc}) = \overleftrightarrow{A}(\hat{\mathbf{n}}^{\rm sca},\hat{\mathbf{n}}^{\rm inc})\cdot\hat{\mathbf{n}}^{\rm inc} = \mathbf{0}, \qquad (11)$$

where $\mathbf{0}$ is a zero vector. The scattering dyadic has the dimension of length and describes the scattering of a plane electromagnetic wave in the so-called far-field zone of the object. It follows from equation (10) that the propagation of the scattered electromagnetic wave is away from the object. Furthermore, the electric and magnetic field vectors vibrate in the plane perpendicular to the propagation direction, and their amplitudes decay inversely with distance from the object.

[35] The main convenience of the far-field approximation is that it allows one to treat the entire object essentially as a point source of scattered radiation and reduces the scattered field to a simple outgoing spherical wave (Figure 2b). Furthermore, equation (11) shows that only four out of the nine components of the scattering dyadic are independent in the spherical polar coordinate system centered at the origin (Figure 3a). It is therefore convenient to introduce the 2×2 so-called amplitude scattering matrix $\mathbf{S}$ that describes the transformation of the θ and φ components of the incident plane wave into the θ and φ components of the scattered spherical wave:

$$\mathbf{E}^{\rm sca}(r\hat{\mathbf{n}}^{\rm sca}) = \frac{\exp(ik_1 r)}{r}\mathbf{S}(\hat{\mathbf{n}}^{\rm sca},\hat{\mathbf{n}}^{\rm inc})\mathbf{E}_0^{\rm inc}. \qquad (12)$$

Here E denotes a two-element column formed by the θ and φ components of the electric field vector:

$$\mathbf{E} = \begin{bmatrix} E_\theta \\ E_\varphi \end{bmatrix}; \qquad (13)$$

$\theta \in [0,\ \pi]$ is the polar (zenith) angle measured from the positive z axis; and $\varphi \in [0, 2\pi)$ is the azimuth angle measured from the positive x axis in the clockwise direction

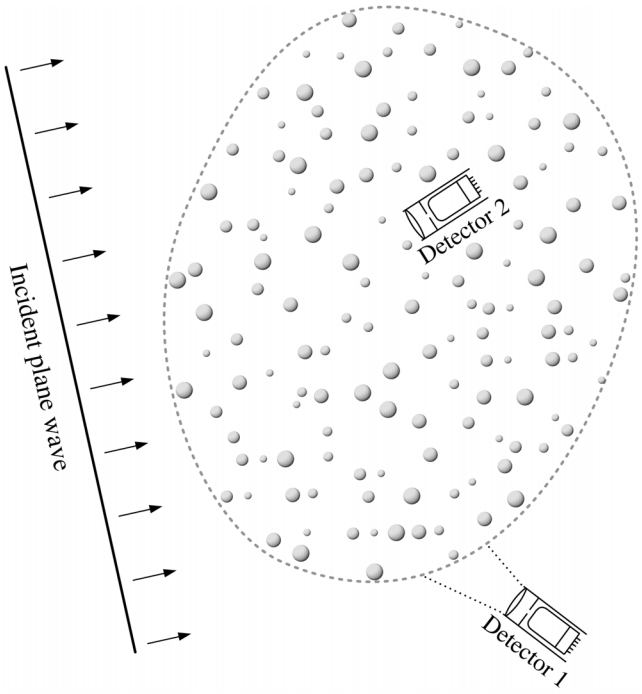

Figure 4. Near-field scattering by a multiparticle group.

when looking in the direction of the positive z axis (Figure 3b). The amplitude scattering matrix has the dimension of length and depends on the incidence and scattering directions as well as on the size, morphology, composition, and orientation of the scattering object with respect to the coordinate system. It also depends on the choice of the origin of the coordinate system relative to the object. If known, the amplitude scattering matrix yields the scattered and thus the total field, thereby providing a complete description of the scattering pattern in the far-field zone.

[36] The conditions defining the far-field zone are as follows [*Mishchenko et al.*, 2006a]:

$$k_1(r-a) \gg 1, \tag{14}$$

$$r \gg a, \tag{15}$$

$$r \gg \frac{k_1 a^2}{2}, \tag{16}$$

where a is the radius of the smallest circumscribing sphere of the entire scattering object centered at O. These conditions are often satisfied for sufficiently small ($k_1 a \lesssim 10^4$) isolated single-particle scatterers. The exact or approximate computation of the amplitude scattering matrix for such particles from the Maxwell equations is also often possible, which explains the widespread use of the amplitude scattering matrix as a single-particle electromagnetic characteristic.

[37] However, there are many important cases in which the conditions (14)–(16) are grossly violated. A good example is remote sensing of water clouds in the terrestrial atmosphere using detectors of electromagnetic radiation mounted on aircraft or satellite platforms. Such detectors typically measure radiation coming from a small part of a cloud and do not "perceive" the entire cloud as a single point-like scatterer (detector 1 in Figure 4). Furthermore, the notion of the far-field zone of the cloud becomes completely meaningless if a detector is placed inside the cloud (detector 2). It is thus clear that to model theoretically the response of such detectors, one has to use scattering characteristics other than the scattering dyadic or the amplitude scattering matrix.

[38] To conclude this section, we note that important early contributions to the subject of far-field electromagnetic scattering were made by *Silver* [1949] and *Müller* [1957].

6. ACTUAL OBSERVABLES

[39] Because of high frequency of the time-harmonic oscillations, traditional optical instruments cannot measure the electric and magnetic fields associated with the incident and scattered waves. Indeed, it follows from

$$\frac{1}{T}\int_t^{t+T} \mathrm{d}t' \, \exp(-\mathrm{i}\omega t') \underset{T \gg 2\pi/\omega}{=} 0 \tag{17}$$

that accumulating and averaging a signal proportional to the electric or the magnetic field over a time interval T long compared with the period of oscillations would yield a zero net result. Therefore, optical instruments usually measure quantities that have the dimension of energy flux and are defined in such a way that the time-harmonic factor $\exp(-\mathrm{i}\omega t)$ vanishes upon multiplication by its complex conjugate counterpart: $\exp(-\mathrm{i}\omega t)[\exp(-\mathrm{i}\omega t)]^* \equiv 1$. This means that in order to make the theory applicable to analyses of actual optical observations, the scattering phenomenon must be characterized in terms of carefully chosen derivative quantities that can be measured directly. This explains the key importance of the concept of an actual observable to the discipline of light scattering by particles.

[40] Although one can always define the magnitude and the direction of the electromagnetic energy flux at any point in space in terms of the Poynting vector [*Jackson*, 1999], the latter carries no information about the polarization state of the incident and scattered fields. The conventional approach to ameliorate this problem dates back to *Stokes* [1852]. He proposed using four real-valued quantities, I, Q, U, and V, which have the dimension of monochromatic energy flux (W m^{-2}) and fully characterize a transverse electromagnetic wave inasmuch as it is subject to practical optical analysis. (By definition, the electric and magnetic field vectors of a transverse electromagnetic wave vibrate in the plane perpendicular to the propagation direction.) These quantities, called the Stokes parameters, form the so-called four-element Stokes column vector $\mathbf{I}$ and carry information about both the total intensity I and the polarization state of the wave.

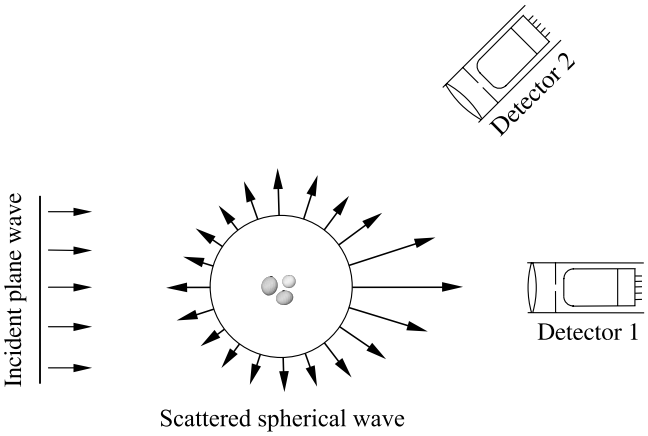

Figure 5. Definition of the extinction and phase matrices.

[41] In the case of far-field scattering, the transversality of both the incident plane wave and the scattered spherical wave allows one to define the corresponding sets of Stokes parameters:

$$\mathbf{I}^{\rm inc}=\begin{bmatrix} I^{\rm inc}\\ Q^{\rm inc}\\ U^{\rm inc}\\ V^{\rm inc}\end{bmatrix}=\frac{1}{2}\sqrt{\frac{\epsilon_1}{\mu_0}}\begin{bmatrix} E_{0\theta}^{\rm inc}\left(E_{0\theta}^{\rm inc}\right)^* + E_{0\varphi}^{\rm inc}\left(E_{0\varphi}^{\rm inc}\right)^*\\ E_{0\theta}^{\rm inc}\left(E_{0\theta}^{\rm inc}\right)^* - E_{0\varphi}^{\rm inc}\left(E_{0\varphi}^{\rm inc}\right)^*\\ -E_{0\theta}^{\rm inc}\left(E_{0\varphi}^{\rm inc}\right)^* - E_{0\varphi}^{\rm inc}\left(E_{0\theta}^{\rm inc}\right)^*\\ {\rm i}\left[E_{0\varphi}^{\rm inc}\left(E_{0\theta}^{\rm inc}\right)^* - E_{0\theta}^{\rm inc}\left(E_{0\varphi}^{\rm inc}\right)^*\right]\end{bmatrix}, \tag{18}$$

$$\mathbf{I}^{\rm sca}(r\hat{\mathbf{n}}^{\rm sca})=\begin{bmatrix} I^{\rm sca}\\ Q^{\rm sca}\\ U^{\rm sca}\\ V^{\rm sca}\end{bmatrix}$$

$$=\frac{1}{r^2}\frac{1}{2}\sqrt{\frac{\epsilon_1}{\mu_0}}\begin{bmatrix} E_{1\theta}^{\rm sca}\left(E_{1\theta}^{\rm sca}\right)^* + E_{1\varphi}^{\rm sca}\left(E_{1\varphi}^{\rm sca}\right)^*\\ E_{1\theta}^{\rm sca}\left(E_{1\theta}^{\rm sca}\right)^* - E_{1\varphi}^{\rm sca}\left(E_{1\varphi}^{\rm sca}\right)^*\\ -E_{1\theta}^{\rm sca}\left(E_{1\varphi}^{\rm sca}\right)^* - E_{1\varphi}^{\rm sca}\left(E_{1\theta}^{\rm sca}\right)^*\\ {\rm i}\left[E_{1\varphi}^{\rm sca}\left(E_{1\theta}^{\rm sca}\right)^* - E_{1\theta}^{\rm sca}\left(E_{1\varphi}^{\rm sca}\right)^*\right]\end{bmatrix}. \tag{19}$$

Then the response of a well-collimated polarization-sensitive detector of light can be described in terms of the 4×4 so-called phase and extinction matrices.

[42] Specifically, detector 2 in Figure 5 collects only the scattered light, and its polarized reading is fully characterized by the product of the phase matrix $\mathbf{Z}$ and the Stokes column vector of the incident wave:

$$\textbf{Signal 2}=\Delta S\mathbf{I}^{\rm sca}(r\hat{\mathbf{n}}^{\rm sca})=\frac{\Delta S}{r^2}\mathbf{Z}\left(\hat{\mathbf{n}}^{\rm sca},\hat{\mathbf{n}}^{\rm inc}\right)\mathbf{I}^{\rm inc},\qquad \hat{\mathbf{n}}^{\rm sca}\neq\hat{\mathbf{n}}^{\rm inc}, \tag{20}$$

where ΔS is the area of the sensitive surface of the detector. Thus the phase matrix realizes the transformation of the Stokes parameters of the incident wave into the Stokes parameters of the scattered wave. The elements of the phase matrix have the dimension of area and are quadratic combinations of the elements of the amplitude scattering matrix $\mathbf{S}(\hat{\mathbf{n}}^{\rm sca},\hat{\mathbf{n}}^{\rm inc})$ [*Mishchenko et al.*, 2002].

[43] Unlike detector 2, detector 1 is facing the incident light, and its polarized reading consists of three parts: (1) the one due to the incident light; (2) the one due to the forward scattered light; and (3) the one due to the interference of the incident wave and the wave scattered by the object in the exact forward direction:

$$\textbf{Signal 1}=\int_{\Delta S}dS\mathbf{I}(r\hat{\mathbf{r}})$$
$$=\Delta S\mathbf{I}^{\rm inc}+\frac{\Delta S}{r^2}\mathbf{Z}\left(\hat{\mathbf{n}}^{\rm inc},\hat{\mathbf{n}}^{\rm inc}\right)\mathbf{I}^{\rm inc}-\mathbf{K}\left(\hat{\mathbf{n}}^{\rm inc}\right)\mathbf{I}^{\rm inc} \tag{21}$$

$$\textbf{Signal 1}=\Delta S\mathbf{I}^{\rm inc}+\boldsymbol{O}\left(r^{-2}\right)-\mathbf{K}\left(\hat{\mathbf{n}}^{\rm inc}\right)\mathbf{I}^{\rm inc}, \tag{22}$$

where $\boldsymbol{O}(r^{-2})$ is a 4×4 matrix with elements vanishing at infinity as r^{-2} [*Mishchenko et al.*, 2002]. The third part is described by minus the product of the extinction matrix $\mathbf{K}$ and the Stokes column vector of the incident wave. The elements of the extinction matrix have the dimension of area and are linear combinations of the elements of the forward scattering amplitude matrix $\mathbf{S}(\hat{\mathbf{n}}^{\rm inc},\hat{\mathbf{n}}^{\rm inc})$ [*Mishchenko et al.*, 2002]. Equations (21) and (22) represent the most general form of the so-called optical theorem.

[44] The situation depicted in Figure 5 is, in many respects, the embodiment of the concept of light scattering. Indeed, it demonstrates that in the absence of the object, detector 2 would measure no signal, while the signal measured by detector 1 would be proportional to the Stokes column vector of the incident light. In the presence of the object, the readings of both detectors change. The reading of detector 2 is now proportional to the Stokes column vector of the scattered field, while the polarization signal measured by detector 1 is modified in two ways. First, the total measured intensity is attenuated as a combined result of the scattering of electromagnetic energy by the object in all directions and, possibly, the transformation of electromagnetic energy into other forms of energy (such as heat) inside the object. Second, the modification rates for the four Stokes components of the measured signal can be different. This effect is typical of objects lacking perfect spherical symmetry and is called dichroism. Thus, to describe far-field scattering means, in effect, to quantify the differences between the readings of detectors 1 and 2 in the presence of the object and in the absence of the object. This quantification can be fully achieved in terms of the phase and extinction matrices that depend on object characteristics such as size, shape, refractive index, and orientation and can be readily computed provided that the amplitude scattering matrix is known.

[45] The near field is not, in general, a transverse electromagnetic wave. Therefore, to characterize the response of the "near-field" detectors shown in Figure 4, one must define quantities other than the Stokes parameters and the extinction and phase matrices. Still, the actual observables must be defined in such a way that they can be measured by an optical device ultimately recording the flux of electro-

magnetic energy. We will see in sections 12 and 13 how this is done in the framework of the theories of RT and WL.

7. FOLDY-LAX EQUATIONS

[46] As we have mentioned in section 4, many theoretical techniques based on directly solving the differential Maxwell equations or their integral counterparts are applicable to an arbitrary fixed finite object, be it a single physical body or a cluster consisting of several distinct components, either touching or spatially separated. These techniques are based on treating the object as a single scatterer and yield the total scattered field. However, if the object is a multiparticle group, such as a cloud of water droplets, then it is often convenient to represent the total scattered field as a vector superposition of partial fields scattered by the individual particles. This means that the total electric field at a point $\mathbf{r}$ is written as follows:

$$\mathbf{E}(\mathbf{r}) = \mathbf{E}^{\rm inc}(\mathbf{r}) + \sum_{i=1}^{N} \mathbf{E}_i^{\rm sca}(\mathbf{r}), \qquad \mathbf{r} \in \Re^3, \tag{23}$$

where N is the number of particles in the group and $\mathbf{E}_i^{\rm sca}(\mathbf{r})$ is the ith partial scattered electric field.

[47] The partial scattered fields can be found by solving vector so-called Foldy-Lax equations (FLEs) that follow directly from the VIE and are exact [*Babenko et al.*, 2003; *Mishchenko et al.*, 2006a]. Specifically, the ith partial scattered field is given by

$$\mathbf{E}_i^{\rm sca}(\mathbf{r}) = \int_{V_i} d\mathbf{r}' \quad \ddot{G}(\mathbf{r}, \mathbf{r}') \cdot \int_{V_i} d\mathbf{r}'' \quad \ddot{T}_i(\mathbf{r}', \mathbf{r}'') \cdot \mathbf{E}_i(\mathbf{r}''), \tag{24}$$

where V_i is the volume occupied by the ith particle, $\mathbf{E}_i(\mathbf{r}'')$ is the electric field "exciting" particle i, and the N dyadics $\ddot{T}_i$ can be found by solving individually the following Lippmann-Schwinger equation:

$$\begin{aligned}\overleftrightarrow{T}_i(\mathbf{r}, \mathbf{r}') = {} & k_1^2 \left[m_i^2(\mathbf{r}) - 1\right] \delta(\mathbf{r} - \mathbf{r}') \overleftrightarrow{I} \\ & + k_1^2 \left[m_i^2(\mathbf{r}) - 1\right] \int_{V_i} d\mathbf{r}'' \overleftrightarrow{G}(\mathbf{r}, \mathbf{r}'') \\ & \cdot \overleftrightarrow{T}_i(\mathbf{r}'', \mathbf{r}'), \qquad \mathbf{r}, \mathbf{r}' \in V_i. \end{aligned} \tag{25}$$

Comparison with equation (8) shows that $\ddot{T}_i$ for each i is, in fact, the dyadic transition operator of particle i with respect to the fixed laboratory coordinate system computed in the absence of all the other particles. Thus, the N dyadic transition operators are totally independent of each other. However, the exciting fields are interdependent and must be found by solving the following system of N linear integral equations:

$$\begin{aligned}\mathbf{E}_i(\mathbf{r}) = {} & \mathbf{E}^{\rm inc}(\mathbf{r}) + \sum_{j(\neq i)=1}^{N} \int_{V_j} d\mathbf{r}' \overleftrightarrow{G}(\mathbf{r}, \mathbf{r}') \\ & \cdot \int_{V_j} d\mathbf{r}'' \overleftrightarrow{T}_j(\mathbf{r}', \mathbf{r}'') \cdot \mathbf{E}_j(\mathbf{r}''), \\ & \mathbf{r} \in V_i, \qquad i = 1, \ldots, N. \end{aligned} \tag{26}$$

[48] In general, the FLEs (23)–(26) are equivalent to equations (7) and (8). However, the fact that $\ddot{T}_i$ for each i is an individual property of the ith particle computed as if this particle were alone allows one to introduce the concept of multiple scattering. This will be the subject of section 8.

[49] One specific, numerically exact approach to solve the FLEs is the so-called superposition T matrix method that involves the expansion of the various electric fields in vector spherical wave functions centered either at the common origin of the entire scattering object or at the individual particle origins [*Fuller and Mackowski*, 2000; *Mishchenko et al.*, 2002; *Doicu et al.*, 2006; *Borghese et al.*, 2007]. This technique is especially efficient in application to groups of spherically symmetric particles and will be used in section 11 to illustrate the scattering effects that can and cannot be described by the theories of RT and WL.

8. WHAT IS MULTIPLE SCATTERING?

[50] Let us rewrite equations (23), (24), and (26) in the following compact operator form:

$$E = E^{\rm inc} + \sum_{i=1}^{N} \hat{G}\hat{T}_i E_i, \tag{27}$$

$$E_i = E^{\rm inc} + \sum_{j(\neq i)=1}^{N} \hat{G}\hat{T}_j E_j, \tag{28}$$

where

$$\hat{G}\hat{T}_j E_j = \int_{V_j} d\mathbf{r}' \quad \ddot{G}(\mathbf{r}, \mathbf{r}') \cdot \int_{V_j} d\mathbf{r}'' \quad \ddot{T}_j(\mathbf{r}', \mathbf{r}'') \cdot \mathbf{E}_j(\mathbf{r}''). \tag{29}$$

Iterating equation (28) yields

$$\begin{aligned} E_i = {} & E^{\rm inc} + \sum_{j(\neq i)=1}^{N} \hat{G}\hat{T}_j E^{\rm inc} + \sum_{\substack{j(\neq i)=1 \\ l(\neq j)=1}}^{N} \hat{G}\hat{T}_j \hat{G}\hat{T}_l E^{\rm inc} \\ & + \sum_{\substack{j(\neq i)=1 \\ l(\neq j)=1 \\ m(\neq l)=1}}^{N} \hat{G}\hat{T}_j \hat{G}\hat{T}_l \hat{G}\hat{T}_m E^{\rm inc} + \cdots, \end{aligned} \tag{30}$$

whereas the substitution of equation (30) in equation (27) gives what can be interpreted as an order-of-scattering expansion of the total electric field:

$$E = E^{\rm inc} + E^{\rm sca}, \tag{31}$$

$$\begin{aligned} E^{\rm sca} = {} & \sum_{i=1}^{N} \hat{G}\hat{T}_i E^{\rm inc} + \sum_{\substack{i=1 \\ j(\neq i)=1}}^{N} \hat{G}\hat{T}_i \hat{G}\hat{T}_j E^{\rm inc} \\ & + \sum_{\substack{i=1 \\ j(\neq i)=1 \\ l(\neq j)=1}}^{N} \hat{G}\hat{T}_i \hat{G}\hat{T}_j \hat{G}\hat{T}_l E^{\rm inc} + \cdots. \end{aligned} \tag{32}$$

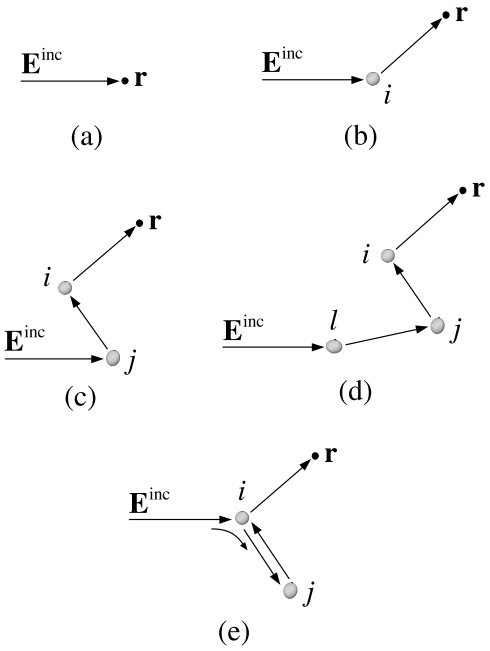

Figure 6. (a) Unscattered (incident) field, (b) single scattering, (c) double scattering, and (d and e) triple scattering.

Indeed, the dyadic transition operators are independent of each other, and each of them can be interpreted as a unique and complete electromagnetic identifier of the corresponding particle. Therefore, $\hat{G}\hat{T}_i E^{\text{inc}}$ can be interpreted as the partial scattered field at the observation point generated by particle i in response to the excitation by the incident field only, $\hat{G}\hat{T}_i\hat{G}\hat{T}_j E^{\text{inc}}$ is the partial field generated by the same particle in response to the excitation caused by particle j in response to the excitation by the incident field, etc. Thus, the first term on the right-hand side of equation (32) can be interpreted as the sum of all single-scattering contributions, the second term is the sum of all double-scattering contributions, etc. The first term on the right-hand side of equation (31) represents the unscattered (i.e., incident) field. This order-of-scattering interpretation of equations (31) and (32) is visualized in Figure 6.

[51] We will see very soon that equations (31) and (32) constitute a very fruitful way of rewriting the original FLEs and that the use of the ''multiple scattering'' terminology is a convenient and compact way of illustrating their numerous consequences. It is important to recognize, however, that besides being an interpretation and visualization tool, the concept of multiple scattering does not represent a physical process per se in the framework of frequency domain electromagnetics. For example, the term $\hat{G}\hat{T}_i\hat{G}\hat{T}_j\hat{G}\hat{T}_l E^{\text{inc}}$ on the right-hand side of equation (32) cannot be interpreted by saying that a light ray (or a localized blob of energy) approaches particle l, gets scattered by particle l toward particle j, approaches particle j, gets scattered by particle j toward particle i, approaches particle i, gets scattered by particle i toward the observation point, and finally arrives at the observation point. Indeed, it follows from equation (26) that all mutual particle-particle excitations occur simultaneously and are not temporally discrete and ordered events. The purely mathematical character of the multiple-scattering interpretation of equation (32) becomes especially apparent upon realizing that this equation is quite general and can be applied not only to a multiparticle group but also to a single body wherein the latter is subdivided arbitrarily into N nonoverlapping adjacent geometrical regions V_i.

[52] It is convenient to represent the order-of-scattering expansion (31)–(32) of the electric field using the diagram method. In Figure 7, the arrows represent the incident field, the line with the circle symbol denotes the ''multiplication'' of a field by a $\hat{G}\hat{T}$ dyadic according to equation (29), and the dashed curve indicates that two scattering ''events'' involve the same particle. The first five terms on the right-hand side of the diagrammatic expression in Figure 7 describe the (cumulative) contributions of the five scattering scenarios, respectively, illustrated in Figure 6.

9. FAR-FIELD FOLDY-LAX EQUATIONS

[53] We have seen in section 5 that as a direct consequence of equations (7) and (9), the behavior of the scattered field becomes much simpler in the far-field zone of the scattering object. Since the structure of equations (24) and (26) is analogous to that of equation (7), one can expect a similar simplification of the FLEs upon making the following two assumptions: (1) The N particles forming the group are separated widely enough that each of them is located in the far-field zones of all the other particles. (2) The observation point is located in the far-field zone of any particle forming the group.

[54] Indeed, the contribution of the jth particle to the field exciting the ith particle in equation (26) can now be represented as a simple outgoing spherical wavelet centered at the origin of particle j. The radius of curvature of this

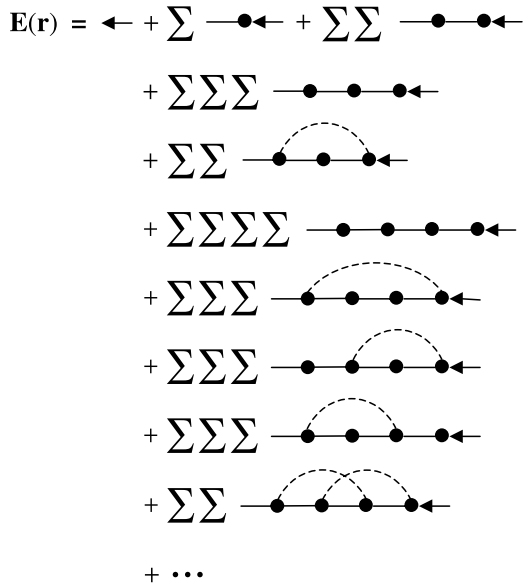

Figure 7. Diagrammatic representation of equations (31) and (32).

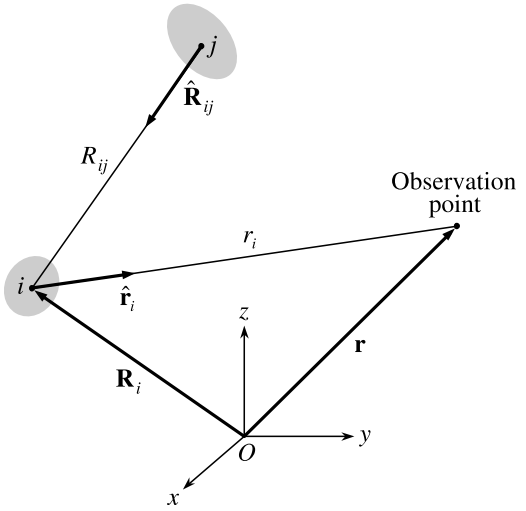

Figure 8. Scattering contribution caused by particle i in response to excitation by particle j.

wavelet at the origin of particle i is much larger than the size of particle i, so that the wavelet can be considered as locally plane. The scattering of this wavelet by particle i can then be described in terms of the corresponding scattering dyadic $\vec{A}_i$ (equation (10)). As a result, the system of integral FLEs turns into a system of algebraic equations [*Mishchenko et al.*, 2006a].

[55] Specifically, assuming that the incident field is a plane electromagnetic wave propagating in the direction $\hat{\mathbf{n}}^{\rm inc}$, we have for the total field at a point $\mathbf{r}$ located in the far-field zone of all the particles:

$$\mathbf{E}(\mathbf{r}) = \mathbf{E}^{\rm inc}(\mathbf{r}) + \sum_{i=1}^{N} G(r_i)\overleftrightarrow{A}_i\left(\hat{\mathbf{r}}_i, \hat{\mathbf{n}}^{\rm inc}\right) \cdot \mathbf{E}^{\rm inc}(\mathbf{R}_i) + \sum_{i=1}^{N} G(r_i) \sum_{j(\neq i)=1}^{N} \overleftrightarrow{A}_i\left(\hat{\mathbf{r}}_i, \hat{\mathbf{R}}_{ij}\right) \cdot \mathbf{E}_{ij}, \tag{33}$$

where $G(r) = \exp(ik_1 r)/r$, r_i is the distance between the origin of particle i and the observation point, $\hat{\mathbf{r}}_i$ is the unit vector directed from the origin of particle i toward the observation point, $\mathbf{R}_i$ is the position vector of the ith particle origin, and $\hat{\mathbf{R}}_{ij}$ is the unit vector directed from the origin of particle j toward the origin of particle i (Figure 8). Equation (33) shows that the total field at any point located sufficiently far from any particle in the group is the superposition of the incident plane wave and N spherical waves generated by and centered at the N particles. The amplitudes of the particle-particle excitations $\mathbf{E}_{ij}$ are found from the following system of $N(N-1)$ linear algebraic equations:

$$\mathbf{E}_{ij} = G\left(R_{ij}\right)\overleftrightarrow{A}_j\left(\hat{\mathbf{R}}_{ij}, \hat{\mathbf{n}}^{\rm inc}\right) \cdot \mathbf{E}^{\rm inc}\left(\mathbf{R}_j\right) + G\left(R_{ij}\right) \sum_{l(\neq j)=1}^{N} \overleftrightarrow{A}_j\left(\hat{\mathbf{R}}_{ij}, \hat{\mathbf{R}}_{jl}\right) \cdot \mathbf{E}_{jl}, \quad i,j = 1,\ldots,N, \qquad j \neq i, \tag{34}$$

where R_{ij} is the distance between the origins of particles j and i.

[56] This system is much simpler than the original system of FLEs and can, in principle, be solved with a computer provided that N is not too large. The expression for the order-of-scattering expansion of the total field also becomes much simpler:

$$\mathbf{E} = \mathbf{E}^{\rm inc} + \sum_{i=1}^{N} \overleftrightarrow{B}_{ri0} \cdot \mathbf{E}_i^{\rm inc} + \sum_{i=1}^{N} \sum_{j(\neq i)=1}^{N} \overleftrightarrow{B}_{rij} \cdot \overleftrightarrow{B}_{ij0} \cdot \mathbf{E}_j^{\rm inc} + \sum_{i=1}^{N} \sum_{j(\neq i)=1}^{N} \sum_{l(\neq j)=1}^{N} \overleftrightarrow{B}_{rij} \cdot \overleftrightarrow{B}_{ijl} \cdot \overleftrightarrow{B}_{jl0} \cdot \mathbf{E}_l^{\rm inc} + \sum_{i=1}^{N} \sum_{j(\neq i)=1}^{N} \sum_{l(\neq j)=1}^{N} \sum_{m(\neq l)=1}^{N} \overleftrightarrow{B}_{rij} \cdot \overleftrightarrow{B}_{ijl} \cdot \overleftrightarrow{B}_{jlm} \cdot \overleftrightarrow{B}_{lm0} \cdot \mathbf{E}_m^{\rm inc} + \cdots, \tag{35}$$

where

$$\mathbf{E} = \mathbf{E}(\mathbf{r}), \qquad \mathbf{E}^{\rm inc} = \mathbf{E}^{\rm inc}(\mathbf{r}), \qquad \mathbf{E}_i^{\rm inc} = \mathbf{E}^{\rm inc}(\mathbf{R}_i), \tag{36}$$

$$\overleftrightarrow{B}_{ri0} = G(r_i)\overleftrightarrow{A}_i\left(\hat{\mathbf{r}}_i, \hat{\mathbf{n}}^{\rm inc}\right), \tag{37}$$

$$\overleftrightarrow{B}_{rij} = G(r_i)\overleftrightarrow{A}_i\left(\hat{\mathbf{r}}_i, \hat{\mathbf{R}}_{ij}\right), \tag{38}$$

$$\overleftrightarrow{B}_{ij0} = G\left(R_{ij}\right)\overleftrightarrow{A}_j\left(\hat{\mathbf{R}}_{ij}, \hat{\mathbf{n}}^{\rm inc}\right), \tag{39}$$

$$\overleftrightarrow{B}_{ijl} = G\left(R_{ij}\right)\overleftrightarrow{A}_j\left(\hat{\mathbf{R}}_{ij}, \hat{\mathbf{R}}_{jl}\right). \tag{40}$$

[57] A remarkable feature of the above formulas is that now the role of the unique electromagnetic identifier of each particle is assumed by the corresponding scattering dyadic, that is, the same quantity that would completely describe far-field scattering by this particle if it were alone rather than a member of the group. Although the dyadic transition operator is the most general scattering property of a particle, the scattering dyadic or, equivalently, the amplitude scattering matrix have been used so frequently to describe far-field scattering by a particle that they have become almost synonymic with the words "single scattering." This appears to add some notoriety to the order-of-scattering interpretation of equation (35). One should not forget, however, that equation (35) is just an approximate version of equations (31) and (32) and does not make multiple scattering a real physical process. The diagrammatic formula shown in Figure 7 can also represent equation (35) provided that the line with the circle symbol is now interpreted as the multiplication of a field by a $\vec{B}$ dyadic.

10. ERGODICITY

[58] Most of our discussion of electromagnetic scattering in sections 4–9 has been based on the assumption that the

configuration of the scattering object with respect to the laboratory reference frame is fixed. However, quite often one has to deal with an object in the form of a multiparticle group in which the particles are randomly rotating and moving relative to each other. The particles may even change their sizes and shapes owing to evaporation, sublimation, condensation, or melting. Important examples of such ''stochastic'' scattering objects are atmospheric clouds consisting of water droplets and/or ice crystals, plumes of aerosol particles, and various particle suspensions. The physical and chemical processes controlling the temporal evolution of such objects can be extremely complex and convoluted.

[59] Although a random group can be described at any given moment in terms of a specific fixed particle configuration, any measurement takes a finite amount of time during which the group goes through an infinite sequence of evolving discrete configurations. Sometimes the result of the measurement can be modeled numerically by solving the Maxwell equations for many time sequential discrete configurations and then taking the average. A far more practical approach in most cases is based on the assumption of ergodicity. Specifically, all further discussion will be based on the following two fundamental premises: (1) The scattering object can be adequately characterized at any moment in time by a finite set of physical parameters. (2) The scattering object is sufficiently variable in time, and the time interval necessary to take a measurement is sufficiently long that averaging the scattering signal over this interval is essentially equivalent to averaging the signal over an appropriate analytical probability distribution of the physical parameters characterizing the scattering object. In other words, we will assume that averaging over time for one specific realization of a random scattering process is equivalent to ensemble averaging.

[60] To better understand the meaning of ergodicity, let us consider the measurement of a scattering characteristic A of a cloud of spherical water droplets. This characteristic depends on time implicitly by being a function of time-dependent physical parameters of the cloud such as the coordinates and radii of all the constituent particles. The full set of particle positions and radii determines the state of the entire cloud at a moment in time and will be denoted collectively by ψ. In order to interpret the measurement of $A[\psi(t)]$ accumulated over a period of time extending from $t = t_0$ to $t = t_0 + T$, one needs a way of predicting theoretically the average value

$$\overline{A} = \frac{1}{T}\int_{t_0}^{t_0+T} dtA[\psi(t)]. \tag{41}$$

[61] As we have already mentioned, the temporal evolution of the cloud of water droplets is described by an intricate system of equations representing the various physical and chemical processes in action. To incorporate the solution of this system of equations for each moment of time into the theoretical averaging procedure (41) can be a formidable task and is never done. Instead, averaging over time is replaced by ensemble averaging based on the following rationale.

[62] Although the coordinates and sizes of water droplets in the cloud change with time in a specific way, the range of instantaneous states of the cloud captured by the detector during the measurement becomes representative of that captured over an infinite period of time provided that T is sufficiently long. We thus have

$$\overline{A} \approx \lim_{\tau\to\infty}\frac{1}{\tau}\int_{t_0}^{t_0+\tau} dtA[\psi(t)] = \langle A\rangle_t. \tag{42}$$

Notice now that the infinite integral in equation (42) can be expected to ''sample'' every physically realizable state ψ of the cloud. Furthermore, this sampling is statistically representative in that the number of times each state is sampled is large and tends to infinity in the limit $\tau \to \infty$. Most importantly, the cumulative contribution of a cloud state ψ to $\langle A\rangle_t$ is independent of the specific moments in time when this state actually occurred in the process of the temporal evolution of the cloud. Rather, it depends on how many times this state was sampled. Therefore, this cumulative contribution can be thought of as being proportional to the probability of occurrence of the state ψ at any moment of time. This means that instead of specifying the state of the cloud at each moment t and integrating over all t, one can introduce an appropriate time-independent probability density function $p(\psi)$ and integrate over the entire physically realizable range of cloud states:

$$\langle A\rangle_t \approx \int d\psi p(\psi)A(\psi) = \langle A\rangle_\psi, \tag{43}$$

where

$$\int d\psi p(\psi) = 1. \tag{44}$$

[63] Equation (43) is the formal mathematical expression of the principle of ergodicity introduced above. Physical processes such as Brownian motion and turbulence often help to establish a significant degree of randomness of particle positions and orientations, which seems to explain why many theoretical predictions based on the ergodic hypothesis have agreed very well with experimental data [*Berne and Pecora*, 1976]. The practical meaning of ergodicity in the framework of the theories of RT and WL will be discussed in section 12.

[64] The ergodic hypothesis was introduced by James Clerk Maxwell (1831–1879) [*Maxwell*, 1879] and Ludwig Boltzmann (1844–1906) as a basic underlying principle of statistical mechanics. The fundamentals of the ergodic theory, its relation to the famous Poincaré recurrence theorem [*Poincaré*, 1890], and its applications to statistical mechanics and kinetic theory are described by *Uhlenbeck and Ford* [1963] and *Farquhar* [1964]. Instructive discussions of the ergodic hypothesis and specific examples of

nonergodic scattering media are given by *Pusey and van Megen* [1989], *Joosten et al.* [1990], *Xue et al.* [1992], *Nisato et al.* [2000], and *Scheffold et al.* [2001].

11. MULTIPLE SCATTERING BY RANDOM PARTICULATE MEDIA: EXACT RESULTS

[65] The far-field order-of-scattering expansion (35) coupled with the principle of ergodicity provides the foundation necessary to develop the microphysical theories of RT and WL. However, before proceeding with the outline of these inherently approximate theories, in this section we will use numerically exact results in order to develop an understanding of what further assumptions and approximations will be necessary and what specific scattering effects these theories may or may not be expected to encompass. To this end, we will analyze T matrix results computed for a macroscopic volume filled with randomly distributed wavelength-sized particles [*Mishchenko et al.*, 2007a]. For practical reasons, the superposition T matrix method cannot be used yet to handle random media consisting of very large numbers of particles such as clouds, colloids, and powder surfaces. However, it does provide the potential to model rather complex particulate systems and thereby simulate the effect of randomness of particle positions as well as the onset and evolution of various "multiple-scattering" effects with increasing number of particles in a statistically homogeneous volume of discrete random medium.

11.1. Static and Dynamic Light Scattering

[66] As we have explained in section 10, in order to simulate measurements of light scattering by a rapidly changing object one needs to solve the Maxwell equations repeatedly for a representative set of distinct object configurations. After the set of solutions of the Maxwell equations has been obtained, one has a choice of (1) analyzing the statistical information content of differences in the individual solutions or (2) applying an averaging procedure and thereby isolating the static component of the scattering pattern. These two approaches are known as dynamic and static light scattering [*Berne and Pecora*, 1976; *Brown*, 1993; *Mishchenko et al.*, 2006a].

11.2. Fixed Configurations of Randomly Positioned Particles: Speckle

[67] Let us assume that a number N of identical spherical particles are distributed randomly throughout a spherical volume V with a radius R much greater than the particle radius a, as shown in Figure 9a. The size parameter of the particles is fixed at $k_1 a = 4$, whereas the size parameter of the spherical volume is fixed at $k_1 R = 40$. The refractive index of the particles relative to that of the surrounding medium is 1.32. The large spherical volume V is illuminated by a plane electromagnetic wave. The incidence direction coincides with the positive direction of the z axis of the laboratory reference frame, and the meridional plane of the incidence direction coincides with the xz half plane with $x \geq 0$ (see Figure 3). The angular distribution and polarization state of the scattered light in the far-field zone of the entire scattering volume is described by the Stokes phase matrix $\mathbf{Z}$ (equation (20)).

[68] Let us first assume that the incident light is circularly polarized in the counterclockwise sense when viewed in the direction of propagation, which implies that $V^{\rm inc} = I^{\rm inc}$ and $Q^{\rm inc} = U^{\rm inc} = 0$. Figures 10a–10d show the far-field angular distributions of the intensity $I^{\rm sca}$ scattered in the backward hemisphere by the large spherical volume filled with $N = 1$, 5, 20, and 80 particles. The individual particle positions were chosen randomly using a random coordinate generator; but otherwise, they are fixed. The scattering pattern for $N = 1$ is rather smooth and perfectly azimuthally symmetric, as it should be for a single wavelength-sized spherical particle. However, Figures 10b–10d demonstrate typical speckle patterns.

[69] The origin of the speckle can be explained as follows. Equations (32) and (9) suggest that at the distant observation point, the partial field due to any particle sequence contributing to the right-hand side of equation (32) becomes an outgoing spherical wavelet centered at the last particle of the sequence. For example, the term $\hat{G}\hat{T}_i\hat{G}\hat{T}_j\hat{G}\hat{T}_l E^{\rm inc}$ becomes a spherical wavelet centered at particle i since the leftmost dyadic Green's function takes the following asymptotic form:

$$\begin{aligned}\overleftrightarrow{G}(\mathbf{r},\mathbf{r}') &= \overleftrightarrow{G}(\mathbf{r}-\mathbf{R}_i,\mathbf{r}'-\mathbf{R}_i)\\ &= \overleftrightarrow{G}(r_i\hat{\mathbf{r}}_i,\mathbf{r}'-\mathbf{R}_i)\underset{r_i\to\infty}{\to}\left(\overleftrightarrow{I}-\hat{\mathbf{r}}_i\otimes\hat{\mathbf{r}}_i\right)\\ &\quad\cdot\frac{\exp(ik_1 r_i)}{4\pi r_i}\exp[-ik_1\hat{\mathbf{r}}_i\cdot(\mathbf{r}'-\mathbf{R}_i)],\qquad \mathbf{r}'\in V_i,\end{aligned}\tag{45}$$

where the notation is explained in Figure 8, and we have made use of the translational invariance property of $\vec{G}$. This occurs irrespective of whether the particles are densely packed or sparsely distributed. The Stokes parameters of the scattered light (equation (19)) can be directly expressed in terms of the elements of the scattering coherency dyad $\vec{\rho}^{\,\rm sca} = \mathbf{E}^{\rm sca}\otimes(\mathbf{E}^{\rm sca})^*$:

$$\mathbf{I}^{\rm sca} = \frac{1}{2}\sqrt{\frac{\epsilon_1}{\mu_0}}\begin{bmatrix}\hat{\boldsymbol{\theta}}^{\rm sca}\cdot\overleftrightarrow{\rho}^{\rm sca}\cdot\hat{\boldsymbol{\theta}}^{\rm sca}+\hat{\boldsymbol{\varphi}}^{\rm sca}\cdot\overleftrightarrow{\rho}^{\rm sca}\cdot\hat{\boldsymbol{\varphi}}^{\rm sca}\\ \hat{\boldsymbol{\theta}}^{\rm sca}\cdot\overleftrightarrow{\rho}^{\rm sca}\cdot\hat{\boldsymbol{\theta}}^{\rm sca}-\hat{\boldsymbol{\varphi}}^{\rm sca}\cdot\overleftrightarrow{\rho}^{\rm sca}\cdot\hat{\boldsymbol{\varphi}}^{\rm sca}\\ -\hat{\boldsymbol{\theta}}^{\rm sca}\cdot\overleftrightarrow{\rho}^{\rm sca}\cdot\hat{\boldsymbol{\varphi}}^{\rm sca}-\hat{\boldsymbol{\varphi}}^{\rm sca}\cdot\overleftrightarrow{\rho}^{\rm sca}\cdot\hat{\boldsymbol{\theta}}^{\rm sca}\\ i\left(\hat{\boldsymbol{\varphi}}^{\rm sca}\cdot\overleftrightarrow{\rho}^{\rm sca}\cdot\hat{\boldsymbol{\theta}}^{\rm sca}-\hat{\boldsymbol{\theta}}^{\rm sca}\cdot\overleftrightarrow{\rho}^{\rm sca}\cdot\hat{\boldsymbol{\varphi}}^{\rm sca}\right)\end{bmatrix},\tag{46}$$

where $\hat{\boldsymbol{\theta}}^{\rm sca}$ and $\hat{\boldsymbol{\varphi}}^{\rm sca}$ are the polar angle and azimuth angle unit vectors such that $\hat{\mathbf{n}}^{\rm sca} = \hat{\boldsymbol{\theta}}^{\rm sca}\times\hat{\boldsymbol{\varphi}}^{\rm sca}$. The dyadic product of the right-hand side of equation (32) and its complex-conjugate counterpart is the sum of an infinite number of terms, each describing the result of interference of two spherical wavelets centered at the end particles of a pair of particle sequences.

[70] One such pair of particle sequences is shown in Figure 9b. If the interference of the corresponding spherical wavelets is constructive (destructive) then it serves to increase (decrease) the total intensity scattered in the direction $\hat{\mathbf{n}}^{\rm sca}$. The total intensity is the sum of the interference

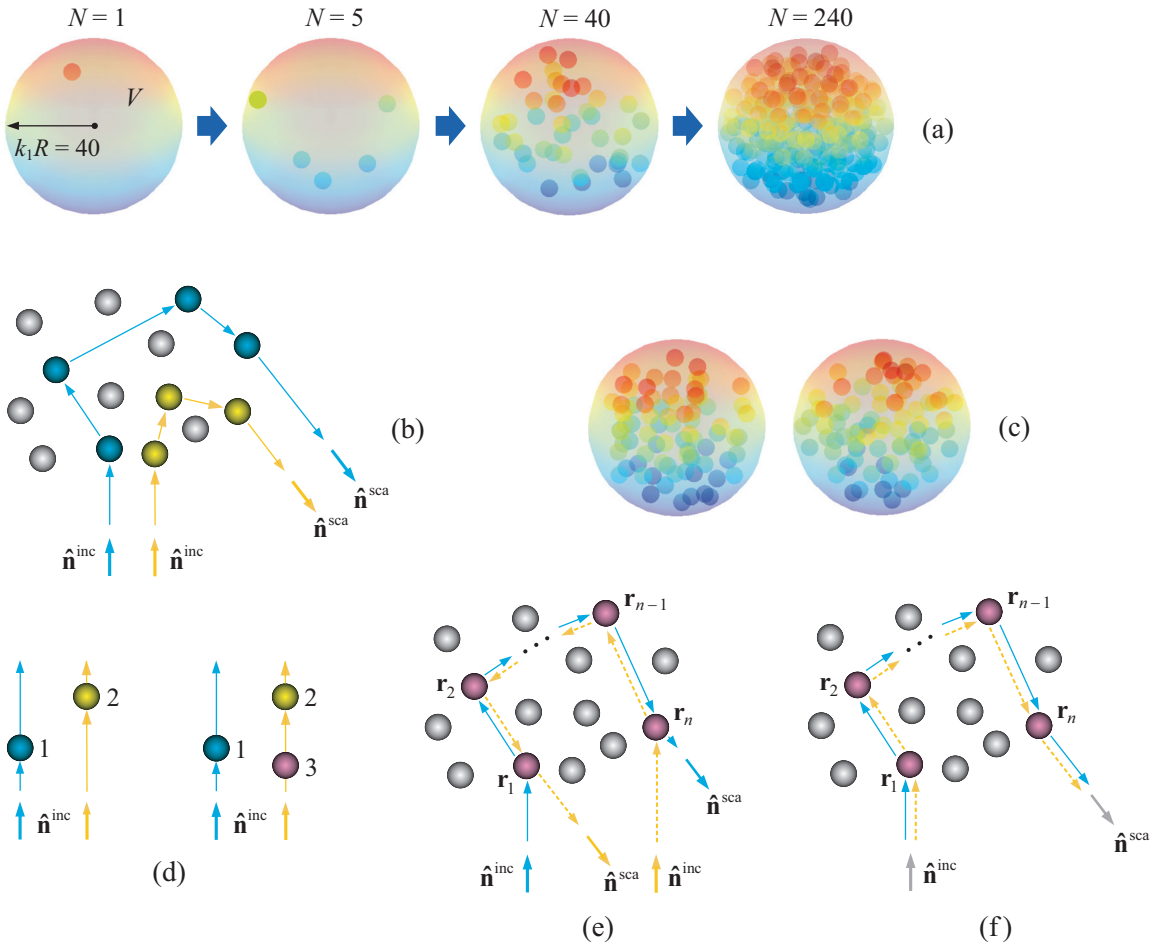

Figure 9. (a) Spherical scattering volume V filled with N randomly positioned particles. (b) Interference origin of speckle. (c) Two random realizations of the 80-particle group. (d) Forward scattering interference. (e) Interference origin of coherent backscattering. (f) Interference origin of the diffuse background.

results contributed by all possible pairs of scattering sequences. The typical angular width of each interference maximum or minimum is proportional to $1/k_1R$, whereas the number of these maxima and minima grows swiftly with increasing N. These two factors explain the spotty appearance of the scattering patterns in Figures 10b–10d.

[71] Of course, the speckle pattern depends not only on the number of particles N but also on the specific way they are arranged with respect to the laboratory coordinate system. This is illustrated by Figures 10d and 10e computed for two different random 80-particle configurations shown in Figure 9c.

11.3. Static Scattering

[72] Figures 10d and 10e illustrate the range of variability of the speckle pattern that can be expected upon even minute changes in a random multiparticle configuration. Obviously, neither the speckle pattern nor its variability are reproduced by the classical theories of RT and WL, which indicates that neither theory describes the instantaneous state of electromagnetic radiation in a discrete random medium. Instead, both theories fall in the realm of static scattering and describe the result of averaging the relevant optical observables over a significant period of time or, equivalently, over a significant range of random particle positions.

[73] To illustrate this fundamental point, one needs an efficient way of averaging the computed scattering signal over very many configurations of the N-particle group. A brute force solution would be to use a random coordinate generator repeatedly to create a large number of different N-particle configurations and then average numerically the corresponding individual T matrix results. The more effective approach used here is to create only one random N-particle configuration and then average over all possible orientations of this configuration with respect to the laboratory coordinate system. This procedure yields an infinite continuous set of random realizations of the N-particle group and takes full advantage of the highly efficient orientation averaging procedure afforded by the

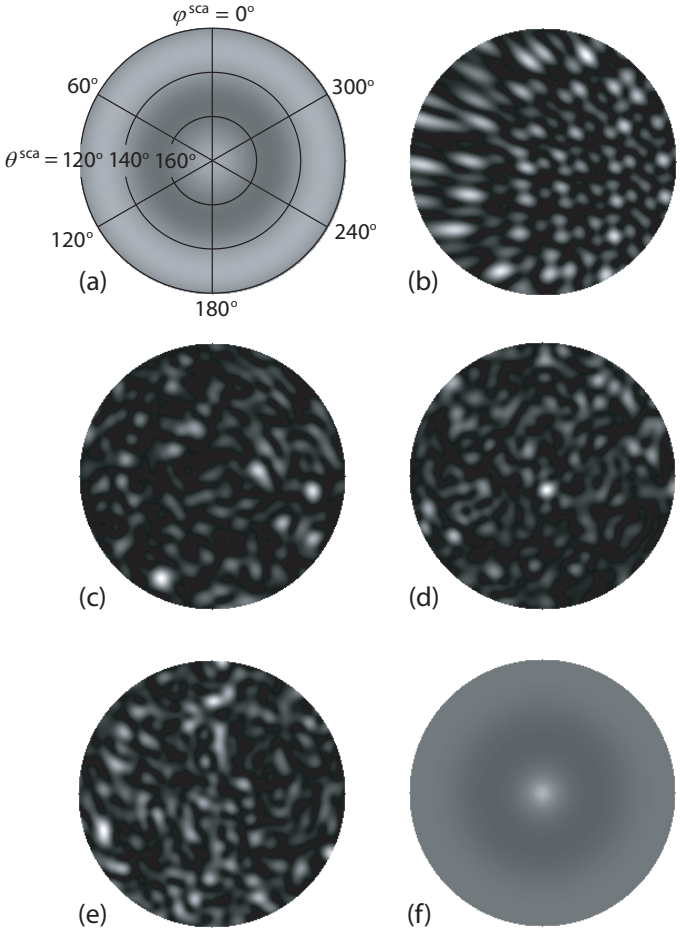

Figure 10. Angular distribution of scattered intensity in the far-field zone of the spherical volume V filled with N particles. (a) $N = 1$, fixed orientation. (b) $N = 5$, fixed orientation. (c) $N = 20$, fixed orientation. (d) and (e) $N = 80$, fixed orientation. (f) $N = 80$, random orientation. The gray scale is individually adjusted in order to maximally reveal the details of each scattering pattern. Figure 10a also shows the angular coordinates used for all images.

superposition T matrix method [*Mackowski and Mishchenko*, 1996; *Mishchenko et al.*, 2002].

[74] Figure 10f shows the result of averaging the speckle pattern over the uniform orientation distribution of the 80-particle configuration used to compute Figure 10d. One can see that with the exception of a notable backscattering peak, the speckle structure is essentially gone. This is not surprising. Indeed, each speckle element is the result of constructive or destructive interference of two wavelets scattered along specific particle sequences such as those shown in Figure 9b. The phase difference between the wavelets changes randomly as the particles move, so that the average result of the interference is zero. However, there are certain pairs of wavelets that interfere constructively irrespective of particle positions and thereby are responsible for the residual scattering pattern. We will demonstrate below that the backscattering intensity peak seen in Figure 10f as well as the smooth intensity background is, in fact, caused by special classes of such wavelet pairs.

[75] In what follows, we employ the concept of multiple scattering to interpret various effects of increasing the number of particles filling the scattering volume on the static scattering patterns obtained by averaging over all orientations of a random N-particle configuration with respect to the laboratory reference frame. We make a simplifying assumption that $\varphi^{sca} = 0$ and define the scattering direction in terms of the scattering angle $\Theta = \theta^{sca}$. Then the scattering process can be conveniently described in terms of the so-called normalized Stokes scattering matrix [*Mishchenko et al.*, 2002, 2006a], which is a particular case of the phase matrix and is given by

$$\tilde{\mathbf{F}}(\Theta) = \begin{bmatrix} a_1(\Theta) & b_1(\Theta) & 0 & 0 \\ b_1(\Theta) & a_2(\Theta) & 0 & 0 \\ 0 & 0 & a_3(\Theta) & b_2(\Theta) \\ 0 & 0 & -b_2(\Theta) & a_4(\Theta) \end{bmatrix}. \quad (47)$$

The specific block-diagonal structure of this matrix [*van de Hulst*, 1957] is confirmed by the numerically exact T matrix results and is largely caused by averaging over the uniform

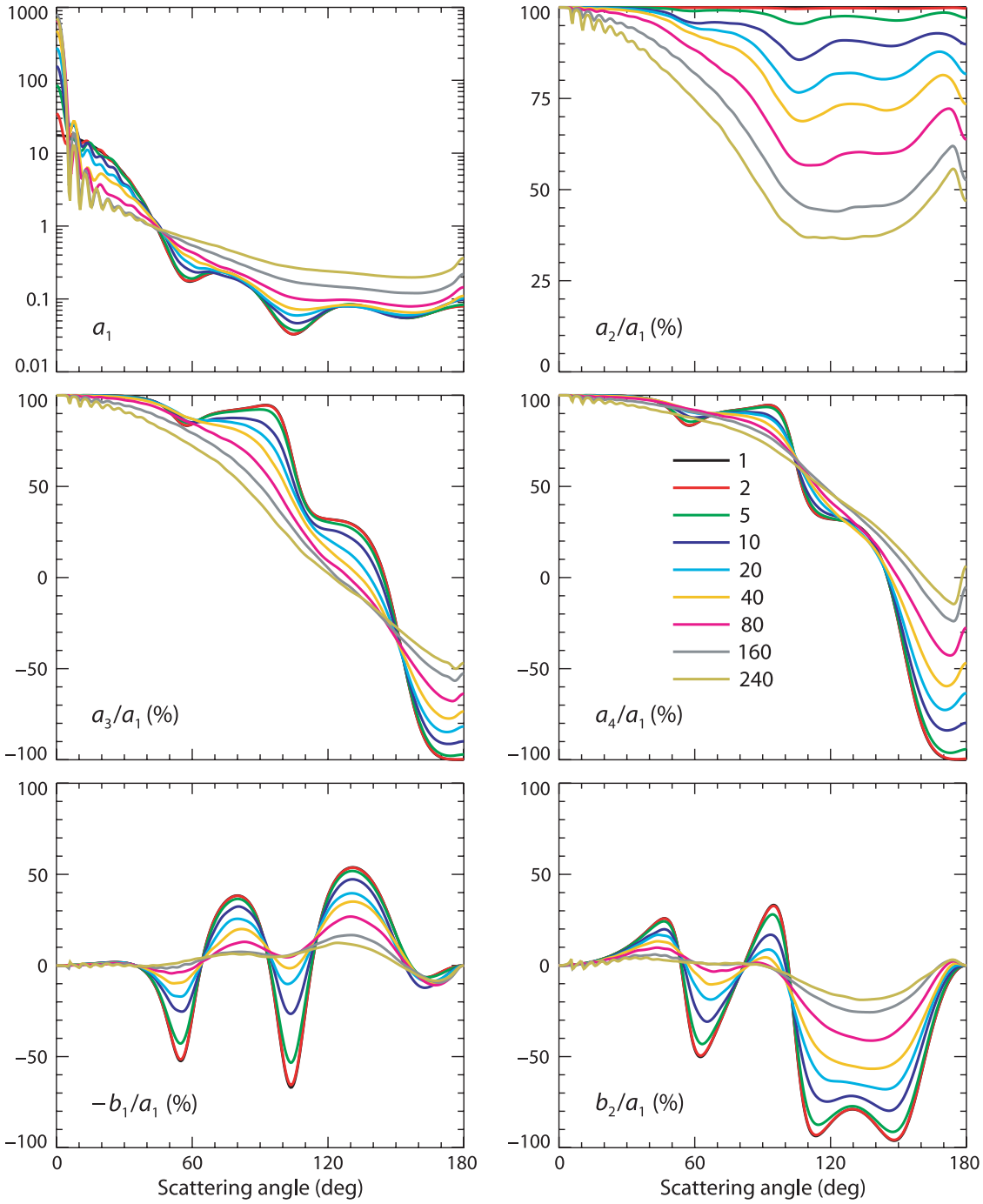

Figure 11. Elements of the normalized Stokes scattering matrix computed for a $k_1R = 40$ spherical volume of discrete random medium filled with $N = 1, \ldots, 240$ particles.

orientation distribution of a multiparticle group coupled with sufficient randomness of particle positions throughout the scattering volume. All scattering matrix elements denoted in equation (47) by a zero have been found to be at least an order of magnitude smaller than the smallest nonzero element (in the absolute value sense). The (1, 1) element, called the phase function, satisfies the following normalization condition:

$$\frac{1}{2}\int_0^\pi d\Theta \sin\Theta a_1(\Theta) = 1. \tag{48}$$

The phase function describes the angular distribution of the scattered intensity provided that the incident light is unpolarized.

[76] The top left-hand plot of Figure 11 vividly demonstrates several fundamental consequences of increasing the number of particles in the scattering volume. First, the constructive interference of light singly scattered by the component particles in the exact forward direction causes a strong forward scattering enhancement [*Mishchenko et al.*, 2006a]. This feature is further detailed in Figure 12a and explained in Figure 9d. It can be called forward scattering

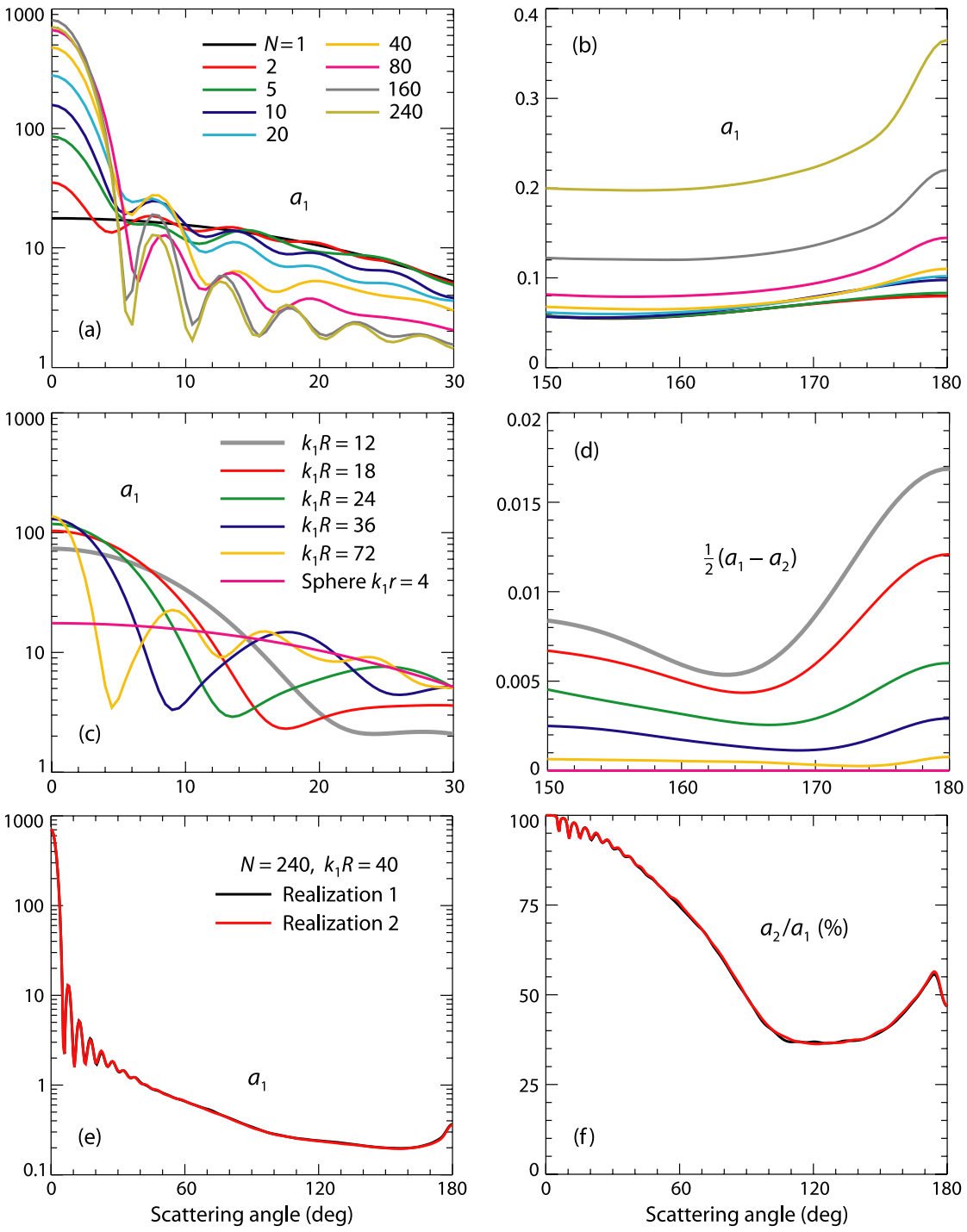

Figure 12. Scattering properties of a spherical volume of discrete random medium.

localization of electromagnetic waves. Indeed, the exact forward scattering direction is unique in that the phase of the wavelets singly forward scattered by all the particles in the volume is exactly the same irrespective of the specific particle positions (see the left-hand plot of Figure 9d). In the absence of multiple scattering, the constructive interference of these wavelets would lead to an increase of the forward scattering phase function $a_1(0^\circ)$ by a factor of N. This increase does occur for $N = 2$ and 5 (Figure 12a), but then it slows down, and by the time N reaches the value 160, the $a_1(0^\circ)$ value saturates. This behavior can be interpreted in terms of a multiple-scattering effect whereby particle 3 (see the right-hand plot of Figure 9d) "shades" particle 2 by attenuating the incident field exciting particle 2. In fact, we will see in section 12 that it is this multiple-scattering effect that leads to the exponential extinction law in the framework of the RT theory.

[77] Second, the phase functions at scattering angles $\Theta > 170^\circ$ start to develop a backscattering enhancement that becomes quite pronounced for $N \geq 160$ (see Figure 12b). This feature is a typical manifestation of WL of electromagnetic waves in the backscattering direction, otherwise

known as the coherent backscattering (CB) effect. (The term ''weak localization of electromagnetic waves'' was introduced by solid-state physicists in order to draw an analogy with the effect of weak localization of electrons in dirty metals [*Sheng*, 2006].) The standard explanation of WL is illustrated in Figure 9e and is as follows: The conjugate wavelets scattered along the same string of n particles but in opposite directions interfere in the far-field zone, the interference being constructive or destructive depending on the respective phase difference,

$$\Delta = k_1(\mathbf{r}_n - \mathbf{r}_1)\cdot\left(\hat{\mathbf{n}}^{\rm inc} + \hat{\mathbf{n}}^{\rm sca}\right). \tag{49}$$

If the observation direction $\hat{\mathbf{n}}^{\rm sca}$ is far from the exact backscattering direction given by $-\hat{\mathbf{n}}^{\rm inc}$, then the average effect of interference of the conjugate wavelets scattered along various strings of particles is zero owing to randomness of particle positions. However, at exactly the backscattering direction, $\hat{\mathbf{n}}^{\rm sca} = -\hat{\mathbf{n}}^{\rm inc}$, the phase difference between the conjugate paths involving any string of particles is identically equal to zero, and the interference is always constructive and causes an intensity peak.

[78] The third consequence of increasing N is that the phase functions at scattering angles $30^\circ \le \Theta \le 170^\circ$ become progressively smooth and featureless, thereby causing the ''diffuse'' intensity background clearly identifiable in Figure 10f. The major contributor to the background intensity is another class of wavelet pairs as illustrated in Figure 9f. Now the wavelet scattered along a string of n particles interferes with itself. Since the corresponding phase difference is exactly equal to zero irrespective of particle positions, the self-interference is always constructive. Therefore, the contribution of this class of wavelet pairs survives the ensemble averaging for any $\hat{\mathbf{n}}^{\rm inc}$ and $\hat{\mathbf{n}}^{\rm sca}$. The smoothness of the background intensity can be interpreted as a typical result of an increasing amount of multiple scattering whereby light undergoing many scattering events ''forgets'' the initial incidence direction $\hat{\mathbf{n}}^{\rm inc}$ and is more likely to contribute equally to all ''exit'' directions $\hat{\mathbf{n}}^{\rm sca}$.

[79] The degree of linear polarization of the scattered light for unpolarized incident light is given by the ratio $-b_1/a_1$. The bottom left-hand plot of Figure 11 shows that the most obvious effect of increasing N is to smooth out the oscillations in the polarization curve for the single wavelength-sized sphere and, on average, to make polarization more neutral. The standard multiple-scattering explanation of this trait is that the main contribution to the second Stokes parameter, $Q^{\rm sca}$, comes from the first order of scattering, whereas light scattered many times (Figure 9f) becomes largely unpolarized.

[80] The ratio a_2/a_1 is identically equal to unity for scattering by a single sphere. Therefore, the rapidly growing deviation of this ratio from 100% for $N \ge 5$ (Figure 11) can again be interpreted as a direct consequence of the strengthened depolarizing effect of multiple scattering. Similarly, $a_3(\Theta) \equiv a_4(\Theta)$ and $a_3(180^\circ)/a_1(180^\circ) = -1$ for single scattering by a spherically symmetric particle, but multiple scattering in particle groups with $N \ge 5$ causes an increasingly significant violation of these equalities.

[81] If the incident light is polarized linearly in the xz plane, then $Q^{\rm inc} = I^{\rm inc}$ and $U^{\rm inc} = V^{\rm inc} = 0$. The corresponding angular distributions of the copolarized,

$$\frac{1}{2}(I^{\rm sca} + Q^{\rm sca}) \propto \frac{1}{2}[a_1(\Theta) + 2b_1(\Theta) + a_2(\Theta)], \tag{50}$$

and cross-polarized,

$$\frac{1}{2}(I^{\rm sca} - Q^{\rm sca}) \propto \frac{1}{2}[a_1(\Theta) - a_2(\Theta)], \tag{51}$$

scattered intensities are shown in Figure 13. Figure 13 also depicts the same helicity,

$$\frac{1}{2}(I^{\rm sca} + V^{\rm sca}) \propto \frac{1}{2}[a_1(\Theta) + a_4(\Theta)], \tag{52}$$

and opposite helicity,

$$\frac{1}{2}(I^{\rm sca} - V^{\rm sca}) \propto \frac{1}{2}[a_1(\Theta) - a_4(\Theta)], \tag{53}$$

scattered intensities for the case of incident light polarized circularly in the counterclockwise direction when looking in the direction of propagation ($Q^{\rm inc} = U^{\rm inc} = 0$ and $V^{\rm inc} = I^{\rm inc}$). All of these quantities exhibit WL in the form of backscattering peaks growing in amplitude with N.

[82] By far, the most definitive demonstration of the onset of the CB effect is provided by the $(a_1 - a_2)/2$ and $(a_1 + a_4)/2$ curves in Figure 13. Indeed, the corresponding single-particle curves show no backscattering enhancement at all, so the backscattering peaks that develop with increasing N (and thus with increasing amount of multiple scattering) can be attributed unequivocally to WL.

[83] Figure 13 also depicts the angular profiles of the so-called linear, $\mu_{\rm L}$, and circular, $\mu_{\rm C}$, polarization ratios defined as the ratio of the cross-polarized to copolarized scattered intensities and the ratio of the same helicity to the opposite helicity scattered intensities:

$$\mu_{\rm L} = \frac{I^{\rm sca} - Q^{\rm sca}}{I^{\rm sca} + Q^{\rm sca}} = \frac{a_1(\Theta) - a_2(\Theta)}{a_1(\Theta) + 2b_1(\Theta) + a_2(\Theta)} \tag{54}$$

$$\mu_{\rm C} = \frac{I^{\rm sca} + V^{\rm sca}}{I^{\rm sca} - V^{\rm sca}} = \frac{a_1(\Theta) + a_4(\Theta)}{a_1(\Theta) - a_4(\Theta)}. \tag{55}$$

These quantities are used widely in radar and lidar remote sensing [*Ulaby and Elachi*, 1990; *Ostro*, 1993; *Stephens*, 1994; *Campbell*, 2002] because they vanish at the exact backscattering direction if multiple scattering is insignificant and the scattering particles are spherically symmetric. Our results demonstrate convincingly that multiple scattering causes an increasingly significant deviation of $\mu_{\rm L}(180^\circ)$ and $\mu_{\rm C}(180^\circ)$ from zero, while WL causes pronounced backscattering peaks in the $\mu_{\rm L}$ and $\mu_{\rm C}$ angular profiles.

[84] The interference mechanism implies that the angular widths of the forward scattering and CB peaks must be

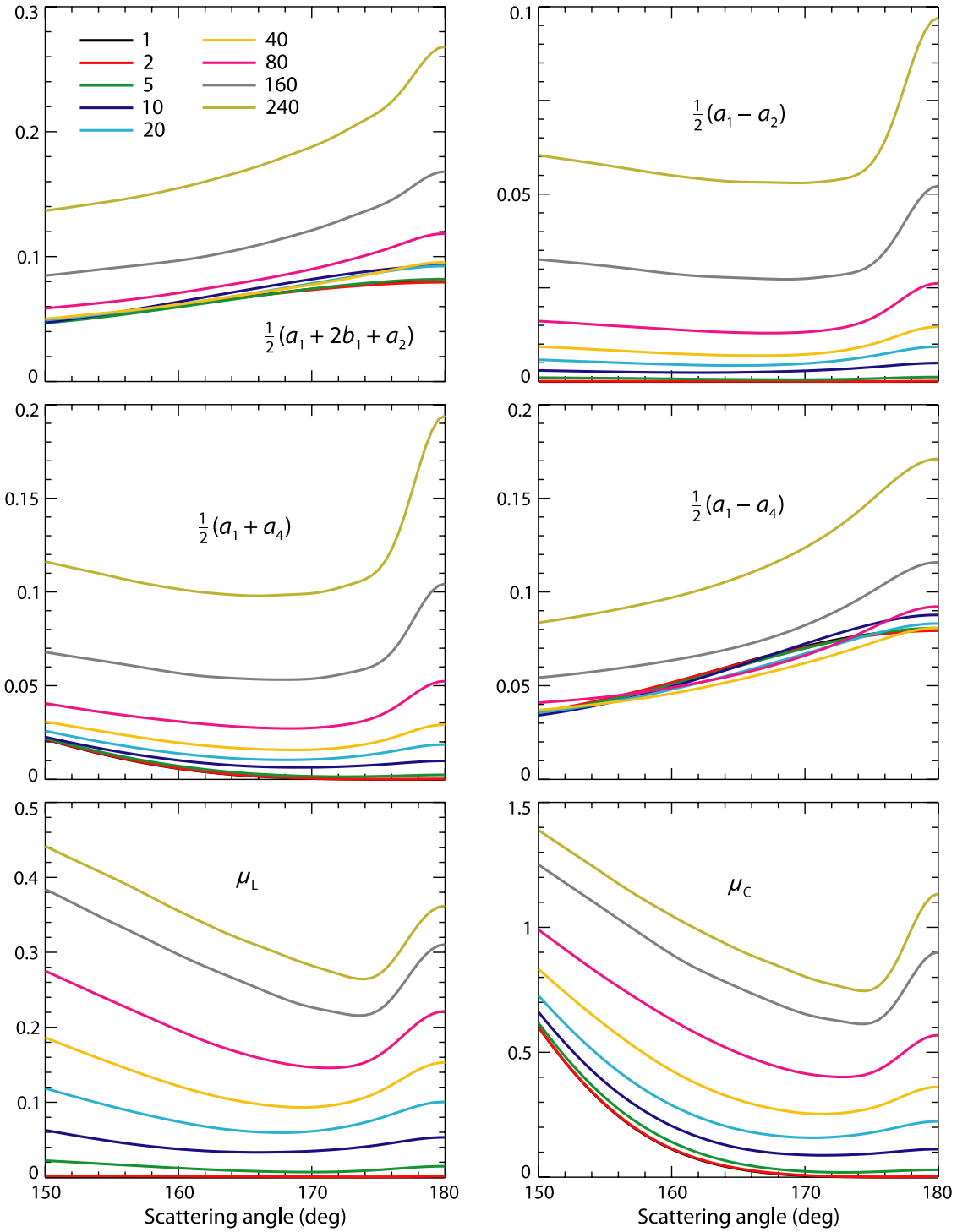

Figure 13. Polarization characteristics of backscattered light computed for a $k_1R = 40$ spherical volume of discrete random medium filled with $N = 1, \ldots, 240$ particles.

inversely proportional to k_1R. To verify this, we have performed computations assuming that the number of $k_1r = 4$ particles is fixed at $N = 8$, whereas the size parameter of the spherical volume is varied from $k_1R = 12$ to 72 in steps of 6. The arrangement of the eight particles inside the $k_1R = 12$ volume is random but such that each particle is in contact with at least one other particle. The other 10 particulate volumes with $k_1R = 18, 24, \ldots, 72$ are obtained by uniformly scaling all particle coordinates of the $k_1R = 12$ volume while keeping the size of the particles fixed. This procedure is illustrated in Figure 14, which shows the original $k_1R = 12$ volume and the derivative $k_1R = 24$ volume. The corresponding T matrix results are depicted in Figures 12c and 12d and demonstrate indeed that the widths of both peaks decrease with increasing interparticle separation, thereby corroborating their interference nature. The nearly constant amplitude of the forward scattering peak and the rapidly decreasing amplitude of the back-

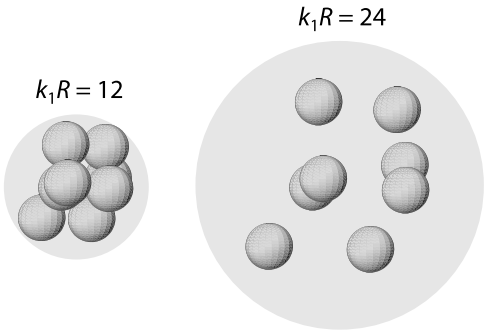

Figure 14. Spherical volumes filled with eight randomly positioned, identical particles.

scattering peak testify again that these features are caused by single and multiple scattering, respectively. Indeed, the single-scattering term does not and the multiple-scattering terms do contain 1/(interparticle distance) factors in the far-field order-of-scattering expansion (35).

[85] Although the results shown in Figures 11–13 are based on averaging over orientations of only one random N-particle configuration, they can be expected to be statistically representative of all possible realizations of the N-particle group at least for large N [*Mishchenko et al.*, 2007a]. This is well demonstrated by Figures 12e and 12f computed for two different realizations of a 240-particle group occupying a $k_1R = 40$ spherical volume.

[86] Thus, the three fundamental classes of wavelet pairs illustrated in Figures 9d–9f are the main contributors to the scattering patterns shown in Figures 10–13. In sections 12 and 13 we will see how and to what extent they are incorporated in the theories of RT and WL.

12. RADIATIVE TRANSFER THEORY

[87] We are now well prepared to proceed with the outline of the RT theory by considering the scattering of a plane electromagnetic wave by a large group of N particles randomly distributed throughout a large 3-D volume V. What follows is a brief sketch of the theory detailed in chapter 8 of *Mishchenko et al.* [2006a].

[88] In accordance with the discussion in sections 9–11, the derivation of the RTE involves several fundamental premises and approximations. The first one is to assume that each particle is located in the far-field zones of all the other particles and that the observation point is also located in the far-field zones of all the particles forming the scattering medium. As we have seen, this assumption leads to a dramatic simplification of the FLEs, wherein the latter are converted from a system of volume integral equations into a system of linear algebraic equations. However, it also limits the applicability of the final result by requiring that the particles in the scattering medium are not closely spaced, a condition that is, nonetheless, met in many natural circumstances.

[89] The order-of-scattering form of the far-field FLEs (equation (35)) allows one to represent the total electric field at a point in space as a sum of contributions arising from light-scattering paths going through all possible particle sequences. The second major assumption, called the Twersky approximation [*Twersky*, 1964; *Mishchenko et al.*, 2006a], is that all paths going through a particle more than once can be neglected. It is straightforward to demonstrate that doing this is justified provided that the number of particles in the scattering volume N is very large. Thus, instead of the diagrammatic equation depicted in Figure 7, we will work with a simplified version depicted in Figure 15.

[90] The third major assumption is that of full ergodicity, which allows one to replace averaging over time by averaging over particle positions and states; see section 10.

[91] The fourth major assumption is that (1) the position and state of each particle are statistically independent of each other and of the positions and states of all the other particles and (2) the spatial distribution of the particles throughout the medium is random and statistically uniform. As one might expect, this assumption leads to a major simplification of all analytical derivations. The practical meaning of ergodicity and uniformity will be discussed at the end of this section.

[92] The next major step is the characterization of the multiply scattered radiation by the coherency dyadic

$$\overleftrightarrow{C}(\mathbf{r}) = \langle \mathbf{E}(\mathbf{r},t) \otimes \mathbf{E}^*(\mathbf{r},t) \rangle_t \approx \langle \mathbf{E}(\mathbf{r}) \otimes \mathbf{E}^*(\mathbf{r}) \rangle_{\mathbf{R},\xi}, \qquad (56)$$

where the subscripts $\mathbf{R}$ and ξ denote averaging over all particle coordinates and states, respectively. The state of a particle can collectively indicate its size, refractive index, shape, orientation, etc. The coherency dyadic is appropriately defined as a nonvanishing quantity; see section 6. Because of the averaging over particle coordinates, $\overleftrightarrow{C}(\mathbf{r})$ is a continuous function of the position vector. Furthermore, as we will see later, the coherency dyadic allows the definition of derivative quantities that are observable directly.

[93] The Twersky expansion of the coherency dyadic is depicted diagrammatically in Figure 16. To classify the different terms entering the expanded expression inside the angular brackets on the right-hand side of this equation, we will use the notation illustrated in Figure 17a. In this particular case, the upper and the lower scattering paths go through different particles. However, the two paths can involve one or more common particles, as shown in Figures 17c and 17d by using the dashed connectors. Furthermore, if the number of common particles is two or more, they can enter the upper and lower paths in the same order, as in Figure 17c, or in the reverse order, as in Figure 17d. Figure 17e shows a mixed diagram in which

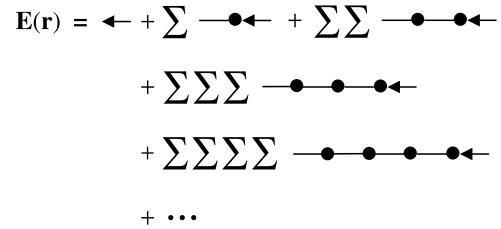

Figure 15. The Twersky approximation.

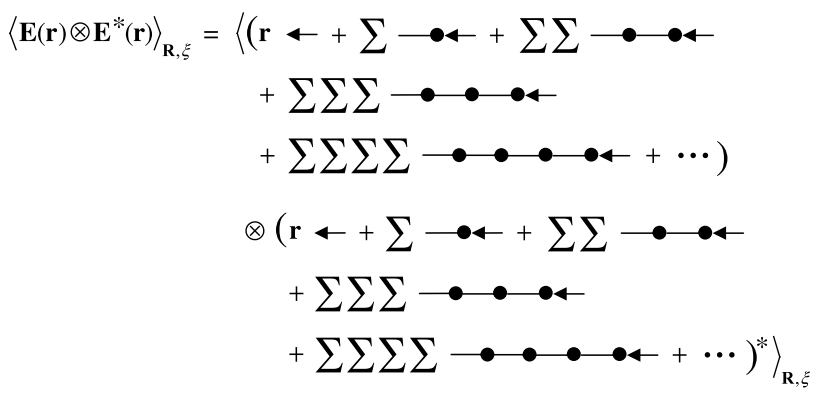

Figure 16. The Twersky expansion of the coherency dyadic.

two common particles appear in the same order and two other common particles appear in the reverse order. The contribution of this diagram to the coherency dyadic is simply

$$\left[\overleftrightarrow{B}_{rij}\cdot\overleftrightarrow{B}_{ijk}\cdot\overleftrightarrow{B}_{jkl}\cdot\overleftrightarrow{B}_{kl0}\cdot\mathbf{E}_l^{\mathrm{inc}}\right]\otimes\left[\overleftrightarrow{B}_{rik}\cdot\overleftrightarrow{B}_{ikj}\cdot\overleftrightarrow{B}_{kjl}\cdot\overleftrightarrow{B}_{jl0}\cdot\mathbf{E}_l^{\mathrm{inc}}\right]^*. \tag{57}$$

By the nature of the Twersky approximation, neither the upper path nor the lower path can go through a particle more than once. Therefore, no particle can be the origin of more than one connector.

[94] The next major assumption in the derivation of the RTE is that all diagrams with crossing connectors can be neglected. The rationale for making this assumption can be illustrated by considering the contribution of the term depicted in Figure 17e to the coherency dyadic. Indeed, by substituting equations (37)–(40) in equation (57), we see that the resulting expression includes a rapidly oscillating exponential factor

$$\exp\left[ik_1\left(R_{ij}+R_{kl}-R_{ik}-R_{jl}\right)\right].$$

This factor causes the contribution of this term to vanish upon averaging over the positions of particles j and k within the volume V provided that all linear dimensions of the volume are much greater than the wavelength of the incident light. However, there is a class of diagrams with crossing connectors that can give a nonvanishing contribution to the coherency dyadic. This class will be discussed in section 13.

[95] Let us now consider the contribution of the diagrams with no crossing connectors like the one shown in Figure 17f. The presence of unconnected particle j in the upper scattering path causes an exponential factor

$$\exp\left[ik_1\left(R_{ij}+R_{jk}\right)\right],$$

which oscillates rapidly everywhere in V except along the straight line connecting the origins of particles i and k, where this factor is constant. The stationary-phase evaluation of the integral describing the average over all positions of particle j yields a very important result: the only effect particle j has in the context of this specific diagram is to attenuate the field generated by particle k and exciting particle i and to potentially cause dichroism. Similarly, particles l, m, and n have any effect only when they all are positioned along the straight line connecting the origins of particles k and o, and this effect is again to cause attenuation and, possibly, dichroism.

[96] Careful analytical evaluation of the cumulative position- and state-averaged contribution of all diagrams with vertical connectors coupled with the assumption that N is very large leads to the equation depicted diagrammatically in Figure 18 [*Mishchenko et al.*, 2006a]. The double-arrow symbol denotes the incident field attenuated by the unconnected particles on its way to the observation point or to the rightmost connected particle, the double lines denote similar attenuation by unconnected particles of a wave propagating from one connected particle to another, and Σ denote both the summation over all appropriate particles and the averaging over the particle positions and states. Owing to their appearance, the diagrams on the right-hand side of this equation are called ladder diagrams. Therefore, this diagrammatic formula can be called the

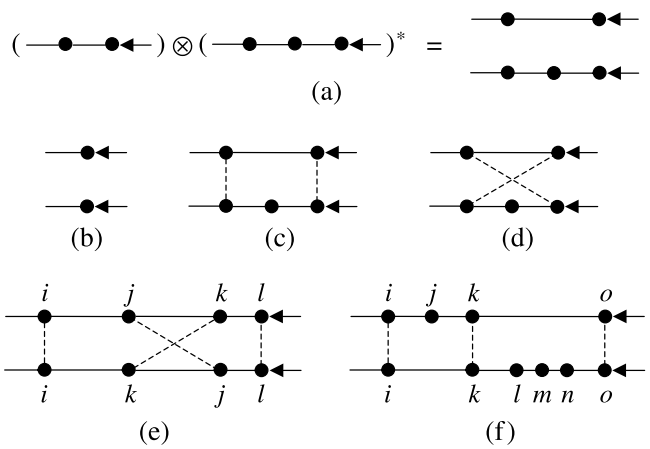

Figure 17. Classification of terms entering the Twersky expansion of the coherency dyadic. (a–c and f) Diagrams with no crossing connectors. (d and e) Diagrams with crossing connectors.

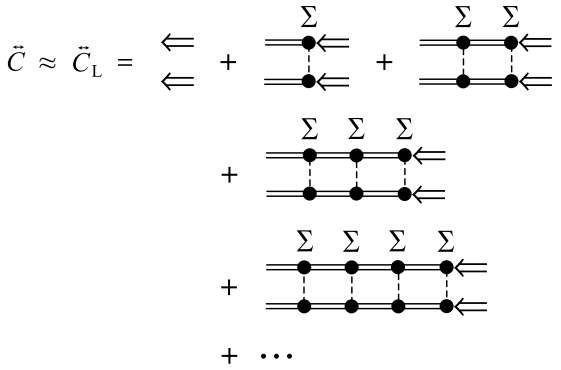

Figure 18. Ladder approximation for the coherency dyadic.

ladder approximation for the coherency dyadic. Obviously, the diagram visualized in Figure 9f and discussed in section 11.3 belongs to the class of ladder diagrams.

[97] The expanded expression for the ladder coherency dyadic has the form of an angular decomposition in terms of the so-called ladder specific coherency dyadic $\vec{\vec{\Sigma}}_{\rm L}(\mathbf{r},\hat{\mathbf{q}})$:

$$\overleftrightarrow{C}_{\rm L}(\mathbf{r}) = \int_{4\pi} d\hat{\mathbf{q}} \overleftrightarrow{\Sigma}_{\rm L}(\mathbf{r},\hat{\mathbf{q}}), \tag{58}$$

where the integration is performed over all propagation directions as specified by the unit vector $\hat{\mathbf{q}}$. Furthermore, it is straightforward to show that the specific coherency dyadic satisfies an integral RTE [*Mishchenko et al.*, 2006a]. The ladder specific coherency dyadic can, in turn, be used to define the so-called specific intensity column vector,

$$\tilde{\mathbf{I}}(\mathbf{r},\hat{\mathbf{q}}) = \begin{bmatrix} \tilde{I}(\mathbf{r},\hat{\mathbf{q}}) \\ \tilde{Q}(\mathbf{r},\hat{\mathbf{q}}) \\ \tilde{U}(\mathbf{r},\hat{\mathbf{q}}) \\ \tilde{V}(\mathbf{r},\hat{\mathbf{q}}) \end{bmatrix}$$

$$= \frac{1}{2}\sqrt{\frac{\epsilon_1}{\mu_0}} \begin{bmatrix} \hat{\boldsymbol{\theta}}(\hat{\mathbf{q}}) \cdot \overleftrightarrow{\Sigma}_{\rm L}(\mathbf{r},\hat{\mathbf{q}}) \cdot \hat{\boldsymbol{\theta}}(\hat{\mathbf{q}}) + \hat{\boldsymbol{\varphi}}(\hat{\mathbf{q}}) \cdot \overleftrightarrow{\Sigma}_{\rm L}(\mathbf{r},\hat{\mathbf{q}}) \cdot \hat{\boldsymbol{\varphi}}(\hat{\mathbf{q}}) \\ \hat{\boldsymbol{\theta}}(\hat{\mathbf{q}}) \cdot \overleftrightarrow{\Sigma}_{\rm L}(\mathbf{r},\hat{\mathbf{q}}) \cdot \hat{\boldsymbol{\theta}}(\hat{\mathbf{q}}) - \hat{\boldsymbol{\varphi}}(\hat{\mathbf{q}}) \cdot \overleftrightarrow{\Sigma}_{\rm L}(\mathbf{r},\hat{\mathbf{q}}) \cdot \hat{\boldsymbol{\varphi}}(\hat{\mathbf{q}}) \\ -\hat{\boldsymbol{\theta}}(\hat{\mathbf{q}}) \cdot \overleftrightarrow{\Sigma}_{\rm L}(\mathbf{r},\hat{\mathbf{q}}) \cdot \hat{\boldsymbol{\varphi}}(\hat{\mathbf{q}}) - \hat{\boldsymbol{\varphi}}(\hat{\mathbf{q}}) \cdot \overleftrightarrow{\Sigma}_{\rm L}(\mathbf{r},\hat{\mathbf{q}}) \cdot \hat{\boldsymbol{\theta}}(\hat{\mathbf{q}}) \\ {\rm i}\left[\hat{\boldsymbol{\varphi}}(\hat{\mathbf{q}}) \cdot \overleftrightarrow{\Sigma}_{\rm L}(\mathbf{r},\hat{\mathbf{q}}) \cdot \hat{\boldsymbol{\theta}}(\hat{\mathbf{q}}) - \hat{\boldsymbol{\theta}}(\hat{\mathbf{q}}) \cdot \overleftrightarrow{\Sigma}_{\rm L}(\mathbf{r},\hat{\mathbf{q}}) \cdot \hat{\boldsymbol{\varphi}}(\hat{\mathbf{q}})\right] \end{bmatrix}, \tag{59}$$

which also satisfies an integral RTE. Finally, the latter can be converted into the following classical integrodifferential form:

$$\hat{\mathbf{q}} \cdot \nabla \tilde{\mathbf{I}}(\mathbf{r},\hat{\mathbf{q}}) = -n_0 \langle \mathbf{K}(\hat{\mathbf{q}}) \rangle_\xi \tilde{\mathbf{I}}(\mathbf{r},\hat{\mathbf{q}}) + n_0 \int_{4\pi} d\hat{\mathbf{q}}' \langle \mathbf{Z}(\hat{\mathbf{q}},\hat{\mathbf{q}}') \rangle_\xi \tilde{\mathbf{I}}(\mathbf{r},\hat{\mathbf{q}}'). \tag{60}$$

In equation (60), $\langle \mathbf{K}(\hat{\mathbf{q}}) \rangle_\xi$ and $\langle \mathbf{Z}(\hat{\mathbf{q}},\hat{\mathbf{q}}') \rangle_\xi$ are the extinction and the phase matrix, respectively, averaged over all particle states, and $n_0 = N/V$ is the particle number density. The specific intensity column vector can be decomposed into the coherent and diffuse parts,

$$\tilde{\mathbf{I}}(\mathbf{r},\hat{\mathbf{q}}) = \delta(\hat{\mathbf{q}} - \hat{\mathbf{n}}^{\rm inc}) \mathbf{I}_{\rm c}(\mathbf{r}) + \tilde{\mathbf{I}}_{\rm d}(\mathbf{r},\hat{\mathbf{q}}), \tag{61}$$

each satisfying its own RTE:

$$\hat{\mathbf{n}}^{\rm inc} \cdot \nabla \mathbf{I}_{\rm c}(\mathbf{r}) = -n_0 \langle \mathbf{K}(\hat{\mathbf{n}}^{\rm inc}) \rangle_\xi \mathbf{I}_{\rm c}(\mathbf{r}), \tag{62}$$

$$\begin{aligned} \hat{\mathbf{q}} \cdot \nabla \tilde{\mathbf{I}}_{\rm d}(\mathbf{r},\hat{\mathbf{q}}) = & -n_0 \langle \mathbf{K}(\hat{\mathbf{q}}) \rangle_\xi \tilde{\mathbf{I}}_{\rm d}(\mathbf{r},\hat{\mathbf{q}}) \\ & + n_0 \int_{4\pi} d\hat{\mathbf{q}}' \langle \mathbf{Z}(\hat{\mathbf{q}},\hat{\mathbf{q}}') \rangle_\xi \tilde{\mathbf{I}}_{\rm d}(\mathbf{r},\hat{\mathbf{q}}') \\ & + n_0 \langle \mathbf{Z}(\hat{\mathbf{q}},\hat{\mathbf{n}}^{\rm inc}) \rangle_\xi \mathbf{I}_{\rm c}(\mathbf{r}). \end{aligned} \tag{63}$$

$\mathbf{I}_{\rm c}$ reduces to the Stokes column vector of the incident wave at the illuminated boundary of the medium but is subject to exponential attenuation and, possibly, the effect of dichroism inside the medium.

[98] The RTE (60) becomes considerably simpler in the case of a plane-parallel, macroscopically isotropic and mirror-symmetric scattering medium [*Hovenier et al.*, 2004; *Mishchenko et al.*, 2006a]:

$$u \frac{d\tilde{\mathbf{I}}(\tau,\hat{\mathbf{q}})}{d\tau} = -\tilde{\mathbf{I}}(\tau,\hat{\mathbf{q}}) + \frac{1}{\langle C_{\rm ext} \rangle_\xi} \int_{4\pi} d\hat{\mathbf{q}}' \langle \mathbf{Z}(\hat{\mathbf{q}},\hat{\mathbf{q}}') \rangle_\xi \tilde{\mathbf{I}}(\tau,\hat{\mathbf{q}}'), \tag{64}$$

where $d\tau = n_0 \langle C_{\rm ext} \rangle_\xi dz$ is the differential element of the optical depth, $\langle C_{\rm ext} \rangle_\xi$ is the average extinction cross section per particle, and $u = -\cos\theta$ is the direction cosine. The z axis of the laboratory right-handed coordinate system is assumed to be perpendicular to the plane boundaries of the medium and directed outward.

[99] The most important corollaries of the microphysical derivation of the RTE are the following [*Mishchenko et al.*, 2006a]:

[100] 1. The derivation of the RTE does not need fundamental physical laws other than those already contained in the classical frequency domain macroscopic electromagnetics. In particular, the ill-defined concepts of collective effects, elementary volume elements, incoherent light rays, and photons as localized particles of light have no relevance whatsoever to the transfer of electromagnetic radiation in elastically scattering discrete random media. It is, in fact, remarkable that although the RTE (60) has the formal mathematical structure of a kinetic equation describing particle transport [*Boltzmann*, 1964], it follows directly from the electromagnetic wave theory.

[101] 2. The RTE is derived by keeping only one class of wavelet pairs, illustrated by Figures 9f and 17f. The effect of unconnected particles is reduced to attenuation and dichroism.

[102] 3. In the context of the RT theory, the scattering properties of particles are specified in terms of the extinction and phase matrices rather than in terms of the scattering

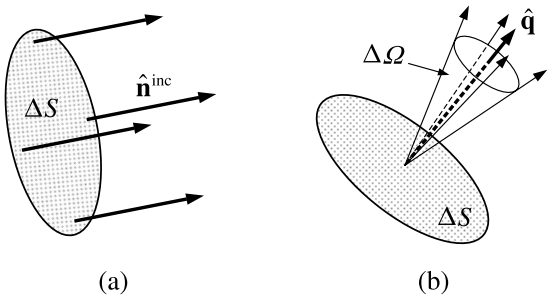

Figure 19. Physical meaning of (a) coherent intensity and (b) specific intensity.

dyadic or the scattering amplitude matrix. Each particle with its individual extinction and phase matrices is effectively replaced with an average particle having the extinction and phase matrices obtained by averaging over all particle states.

[103] 4. In the framework of the exact FLEs, the source of multiple scattering is the constant-amplitude incident field (equation (32)). In the framework of the approximate RT theory, this role is effectively assumed by the exponentially attenuated coherent (or "unscattered") part of the specific intensity column vector described by equation (62).

[104] 5. Averaging over all particle positions makes $\mathbf{I}_{\rm c}$ and $\tilde{\mathbf{I}}_{\rm d}$ continuous functions of the position vector of the observation point $\mathbf{r}$ and also makes $\tilde{\mathbf{I}}_{\rm d}$ a continuous function of the propagation direction $\hat{\mathbf{q}}$.

[105] 6. For the same reason, $\tilde{\mathbf{I}}$ differs from the Stokes column vector of a transverse electromagnetic wave $\mathbf{I}$, in that it has the dimension of monochromatic radiance (W m^{-2} sr^{-1}) rather than the dimension of monochromatic energy flux (W m^{-2}). The reader can see readily that this particular dimension of $\tilde{\mathbf{I}}$ is a direct consequence of the definition (56), the angular decomposition of $\vec{C}_{\rm L}(\mathbf{r})$ according to equation (58), and the definition (59).

[106] 7. The RTE is an inherently vector equation. The frequently used scalar version of the RTE is obtained by artificially replacing the specific intensity vector by its first element (i.e., the specific intensity) and the extinction and phase matrices by their respective (1, 1) elements. As such, the scalar approximation has no compelling physical justification besides being easier to solve and providing acceptable accuracy in many cases [*Mishchenko et al.*, 2006a].

[107] 8. The RTE remains valid if the incident light is a parallel quasi-monochromatic beam.

[108] The integral form of the RTE can be used to clarify the physical meaning of the coherent Stokes column vector $\mathbf{I}_{\rm c}$ and the diffuse specific intensity column vector $\tilde{\mathbf{I}}_{\rm d}$. The fundamental difference between these quantities is that the former describes a monodirectional whereas the latter describes an uncollimated flow of electromagnetic energy (equation (61)). In particular, the first element of the coherent Stokes column vector, i.e., the coherent intensity $I_{\rm c}(\mathbf{r})$, is the electromagnetic power per unit area of a small surface element ΔS perpendicular to the incidence direction $\hat{\mathbf{n}}^{\rm inc}$, whereas the first element of the diffuse specific intensity column vector, i.e., the diffuse specific intensity $\tilde{\mathbf{I}}_{\rm d}(\mathbf{r}, \hat{\mathbf{q}})$, is the electromagnetic power per unit area of a small surface element ΔS perpendicular to $\hat{\mathbf{q}}$ per one steradian of a small solid angle $\Delta\Omega$ centered around $\hat{\mathbf{q}}$ (Figure 19).

[109] This interpretation of $\mathbf{I}_{\rm c}(\mathbf{r})$ and $\tilde{\mathbf{I}}_{\rm d}(\mathbf{r}, \hat{\mathbf{q}})$ implies that both quantities can be measured by appropriately placed and oriented detectors of electromagnetic energy flux. Indeed, the instantaneous direction of the electromagnetic energy flow is given by the Poynting vector and changes rapidly inside a discrete random medium owing to changing particle positions. Therefore, at any given moment in time, a well-collimated detector of electromagnetic energy flux placed inside the medium may or may not register any signal depending on its specific instantaneous orientation. Averaging over time (or, equivalently, over particle positions) ensures that the reading of the detector is always nonzero and is a continuous function of its orientation. The fact that the specific intensity column vector can be both computed theoretically by solving the RTE and measured with a suitable optical device explains the practical usefulness of the RT theory in countless applications in various branches of science and engineering.

[110] Since the microphysical derivation of the RTE involves statistical averaging over particle states and positions, neither the coherent Stokes column vector nor the diffuse specific intensity column vector characterize the instantaneous distribution of the radiation field inside the scattering medium. Instead, they characterize the directional flow of electromagnetic radiation averaged over a sufficiently long period of time. This conclusion is consistent with the discussion in section 11.3. The minimal averaging time necessary to ensure ergodicity may be different for different scattering systems, but the following is always true: the longer the averaging time the more accurate the theoretical prediction based on the RTE. Accumulating a signal over an extended period of time is often used to improve the accuracy of a measurement by reducing the effect of random noise. However, the situation with the RT theory is fundamentally different in that averaging the signal over an extended period of time is necessary to ensure the very applicability of the RTE.

[111] Although the microphysical derivation of the RTE rests on several fundamental premises discussed above, most of them appear to be quite realistic in a great variety of applications. However, the assumptions of ergodicity and spatial uniformity deserve further analysis since they may appear to be too restrictive for the RTE to be useful.

[112] The meaning of the assumptions of ergodicity and uniformity is illustrated in Figure 20. The detector of electromagnetic energy has an angular aperture small enough to resolve the angular variability of the diffuse radiation field (e.g., $\sim 1^\circ$) and a finite acceptance area ΔS. Both define the part of the scattering volume V bounded schematically by the dotted lines in Figure 20; this part will be called the acceptance volume. According to the integral form of the RTE, all energy recorded by the detector comes directly from the particles contained in the acceptance volume. The energy exciting each particle can be either the

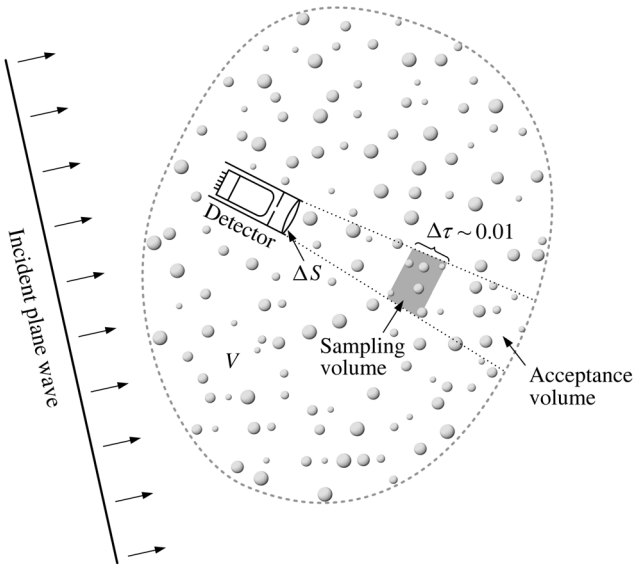

Figure 20. Practical meaning of the assumptions of ergodicity and uniformity.

(attenuated) incident light or the light scattered by the other particles. The light scattered by a particle from the acceptance volume toward the detector can be attenuated by other particles located closer to the detector.

[113] Let us assume that the detector accumulates the signal over a time interval Δt and subdivide the acceptance volume into a number of sampling volumes such that their optical thickness $\Delta\tau$ along the line of sight of the detector is very small ($\sim$0.01). One of these sampling volumes is shown schematically in Figure 20. Obviously, the contribution of a particle to the detector signal is essentially independent of the specific particle position in the sampling volume. Therefore, the strict meaning of the assumptions of ergodicity and statistical uniformity of particle positions within the scattering volume V is that each particle visits each sampling volume during the measurement interval Δt.

[114] In reality, the scattering volume V contains many particles of the same type. Therefore, the practical meaning of ergodicity and uniformity is that particles of each type visit each sampling volume during the measurement interval Δt a number of times statistically representative of the total number of such particles in the entire scattering volume. Obviously, this requirement is significantly softer and can be expected to be met in many actual circumstances.

13. WEAK LOCALIZATION

[115] Consider again a scattering object in the form of a large group of discrete, randomly and sparsely distributed particles (Figure 21). The object is illuminated by a plane electromagnetic wave propagating in the direction $\hat{\mathbf{n}}^{\rm inc}$. The reader should recall that the RTE is derived by neglecting all diagrams with crossing connectors in the diagrammatic representation of the coherency dyadic. Following the line of reasoning outlined in section 12, one may indeed conclude that upon statistical averaging the contribution of all the diagrams of the type illustrated in Figure 22 must vanish at near-field observation points located either inside the object (observation point 1 in Figure 21) or outside the object (observation point 2).

[116] However, we have already discussed in section 11.3 that there is an exception corresponding to the situation when the observation point is in the far-field zone of the scattering object and is located within its "back shadow" (observation point 3 in Figure 21). Then the class of diagrams illustrated by Figure 9e and Figures 22c–22e gives a nonzero contribution that causes the WL effect. These diagrams are called maximally crossed since they can be drawn in such a way that all connectors cross at one point.

[117] The expression for the cumulative contribution of all maximally crossed (or cyclical) diagrams to the coherency dyadic at an observation point can be derived using the diagrammatic technique introduced in section 12. The final result can be summarized by the diagrammatic expression shown in Figure 23. As before, Σ denotes both the summation over all appropriate particles and the statistical averaging over the particle states and positions, whereas the double lines account for the effect of exponential

Figure 21. Scattering of a plane electromagnetic wave by a volume of sparse, discrete random medium.

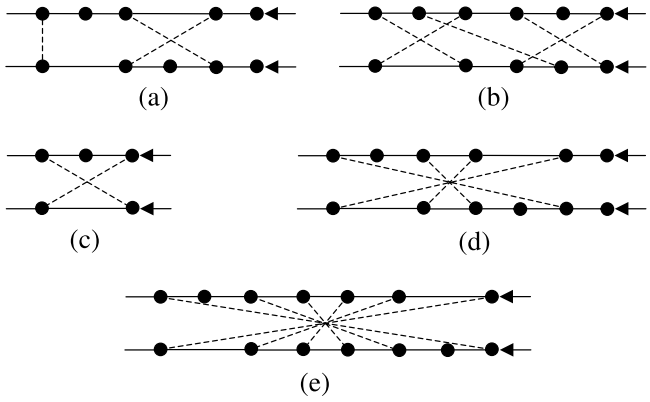

Figure 22. Diagrams with crossing connectors.

attenuation and, possibly, dichroism. It is very instructive to compare Figure 23 with Figure 18 since this comparison reveals quite vividly the morphological difference between the participating diagrams. The total coherency dyadic is now approximated by the following expression:

$$\overleftrightarrow{C} \approx \overleftrightarrow{C}_{\rm L} + \overleftrightarrow{C}_{\rm C}. \tag{65}$$

[118] The inclusion of the cyclical diagrams makes the computation of the coherency dyadic much more involved and limits the range of problems that can be solved accurately. In particular, no closed-form equation similar to the RTE has been derived to describe the CB contribution to the specific coherency dyadic, $\vec{\Sigma}_{\rm C}(\mathbf{r}, \hat{\mathbf{q}})$. However, the reciprocal nature of each single-scattering event leads to an interesting exact result: the characteristics of the CB effect at the exact backscattering direction can be rigorously expressed in terms of the solution of the RTE [*Mishchenko*, 1992]. This result as well as other theoretical and numerical approaches to the problem of WL are reviewed by *Barabanenkov et al.* [1991], *Kuz'min and Romanov* [1996], *van Rossum and Nieuwenhuizen* [1999], *Lenke and Maret* [2000], *Muinonen* [2004], and *Mishchenko et al.* [2006a].

[119] The angular width of the CB effect is inversely proportional to $k_1\langle l\rangle$, where $\langle l\rangle$ is the average distance between the end particles of the various particle sequences such as those shown in Figure 9e. Factors limiting $\langle l\rangle$ and thereby increasing the angular width of the various manifestations of CB are absorption by particles and a finite size of the scattering medium. The finite size effect is well illustrated by Figure 12d. For optically thick media, a good proxy to $\langle l\rangle$ is the so-called transport mean free path $l_{\rm tr}$ [*Ishimaru*, 1978].

[120] The angular width of the various CB features for objects such as water clouds is extremely small and can hardly be observed with passive instruments measuring the scattered sunlight since in this case $l_{\rm tr}$ is many orders of magnitude greater than the wavelength. However, CB can substantially affect the results of active observations of clouds with lidars and radars [e.g., *Kobayashi et al.*, 2007] since these instruments observe electromagnetic radiation scattered in exactly the backscattering direction.

[121] The situation is different for densely packed particulate media, in which case $l_{\rm tr}$ can be comparable to the wavelength of the incident light. As a consequence, CB can be detectable not only with active instruments or specifically designed laboratory equipment [e.g., *Labeyrie et al.*, 2000; *Gross et al.*, 2007; *Psarev et al.*, 2007] but even in telescopic observations of sunlight scattered by surfaces of high-albedo solar system bodies (e.g., *Rosenbush et al.* [2002], *Mishchenko et al.* [2006b], *French et al.* [2007], and references therein). It is important to recognize, however, that the very concept of wave phase applies only to transverse waves such as plane and spherical waves. Therefore, the interference explanation of WL is implicitly based on the assumption that each particle in any particle string (Figure 9e) is located in the far-field zones of the previous and the following particle. This assumption can often be violated in densely packed particulate media. However, the presence of strong CB peaks in the exact T matrix results obtained for 240 densely packed particles (Figures 12b and 13) indicates that the wavelets scattered along strings of widely separated particles still provide a significant contribution to the total scattered signal.

[122] Monostatic radars use the same antenna to transmit and receive electromagnetic waves. Therefore, radar measurements of particulate media are inevitably affected by WL. Several solar system objects have been found to generate radar returns quite uncharacteristic of bare solid surfaces. For example, the icy Galilean satellites of Jupiter exhibit both high radar reflectivities and circular polarization ratios exceeding one [*Ostro*, 1993]. Similar radar echoes have been detected in radar observations of the poles of Mercury [*Harmon et al.*, 1994]. These measurements have been interpreted in terms of multiple scattering, including WL, of electromagnetic waves by voids or rocks imbedded in a transparent layer of ice [*Hapke*, 1993; *Mishchenko et al.*, 2006a].

[123] The interference explanation of WL assumes that the observer is located in the far-field zone of the entire scattering medium. In reality, the various manifestations of CB can be observed at distances shorter than those dictated by equation (16). Specifically, the distance r from the scattering medium to the observation point must satisfy the following inequality [*Mishchenko et al.*, 2006a]:

$$r \gg \frac{1}{2} k_1 \langle l\rangle^2. \tag{66}$$

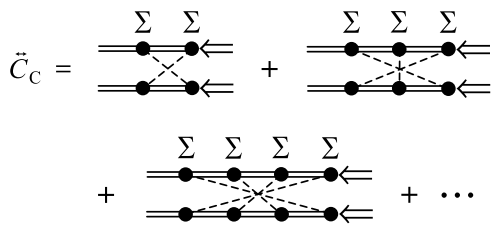

Figure 23. The cyclical part of the coherency dyadic.

However, the requirement (66) can be rather demanding if the scattering medium is composed of nonabsorbing, wavelength-sized or larger particles and its minimal dimension is greater than l_{tr}.

14. FORWARD SCATTERING INTERFERENCE

[124] Similarly to CB, the forward scattering localization of electromagnetic waves discussed in section 11.3 and illustrated in Figure 9d is an expressly far-field scattering effect and as such is not accounted for by the RTE. Indeed, it can be readily shown that the contribution of the diagrams of the type shown in Figure 17b evaluated at a near-field observation point does not vanish only when both particles are positioned along the same straight line parallel to the incidence direction and going through the observation point. This nonvanishing contribution is ultimately included in the exponentially attenuated coherent Stokes column vector $\mathbf{I}_c$.

[125] In order to observe the forward scattering interference effect directly, the observation point must be located in the far-field zone, i.e., at a distance r from the scattering volume satisfying the inequalities (14)–(16). This factor makes the RTE a rather robust approximation. To appreciate this point, one can apply equation (16) to a small cloud of water droplets with a typical dimension of 100 m assuming that the incident wavelength is 500 nm. Simple arithmetic then yields $r \gg 10^{10}$ m.

15. WHAT IS INDEPENDENT SCATTERING?

[126] We have seen before that at any moment in time, the incident electromagnetic wave perceives the entire multiparticle group as a unified, albeit morphologically complex, scatterer. We have also witnessed how the RTE emerges from the Maxwell equations as a consequence of several assumptions (such as wide interparticle separation) and, in the final analysis, contains (ensemble averaged) single-particle extinction and phase matrices. However, a traditional (and incorrect!) way of dealing with the problem of multiple scattering and RT has been to proceed in the opposite direction: by first considering widely separated, randomly positioned particles as ''independent scatterers,'' then assigning to them individual extinction and phase matrices, then considering ''incoherent'' single and multiple scattering by the ''independently scattering particles,'' and finally speculating how the individual scattering properties of the particles can change as a consequence of various ''packing density'' effects.

[127] It is thus clear that the notion of ''independent scattering'' has been very important to the discipline of light scattering by particle groups. Several definitions of ''independently scattering particles'' have been given in the literature (e.g., *van de Hulst* [1957], *Cartigny et al.* [1986], *Tien* [1988], *Kumar and Tien* [1990], *Ivezić and Mengüç* [1996], *Liou* [2002], *Mishchenko et al.* [2002, 2006a], *Martin* [2006], and references therein). Some of these definitions may be rather vague, and some of them actually refer to what is otherwise known as the ''single-scattering approximation'' relevant to the case of scattering by a small group of widely separated particles [*Agarwal and Mengüç*, 1991; *Mishchenko et al.*, 2006a, 2007b]. (It should be kept in mind that the specific conditions of applicability of the single-scattering and RT approximations in terms of the minimal average interparticle separation can be somewhat different [*Mishchenko et al.*, 2006a].) The common intent of these definitions has been to ensure that observable consequences of scattering by a multiparticle group are ultimately described in terms of the extinction and phase matrices of the individual particles, i.e., the quantities describing single-particle transformations of Stokes parameters rather than electric fields.

[128] The microphysical approach outlined above makes it quite clear that a particle is an independent scatterer only when it is completely alone. Particles forming a group cannot be independent scatterers irrespective of how widely they are separated and how randomly they are distributed since the forward scattering interference and CB effects are ubiquitous and cannot be described in terms of individual particle extinction and phase matrices. In the case of large rarefied objects such as terrestrial water clouds, the forward scattering and CB intensity peaks are extremely narrow, contain a negligible fraction of the total scattered energy, and are hardly observable, thereby making the RT theory a very good quantitative descriptor of many actual observables. We have seen, however, that even in the limited context of the RT theory, particles are not characterized by their individual extinction and phase matrices. Instead, each particle is replaced by an ''average'' particle characterized by the ensemble-averaged extinction and phase matrices.

[129] We must therefore conclude that the term ''independent scattering'' has little heuristic value and can, in fact, be quite misleading. Perhaps the least ambiguous, albeit still undesirable, way to use this term is in application to randomly positioned particles located in the far-field zones of each other, since the randomness and far-field conditions are necessary in the theories of RT and WL.

16. RADIATIVE TRANSFER IN GASEOUS MEDIA

[130] It is well known that multiple scattering can be caused not only by particles but also by density and anisotropy fluctuations in rarefied molecular media such as gases [*von Smoluchowski*, 1908]. This type of scattering is traditionally called Rayleigh scattering and is thoroughly reviewed by *Fabelinskii* [1968] and *Kuz'min et al.* [1994]. Each density and/or anisotropy fluctuation can be considered a particle in the sense of causing the electric permittivity (or, in general, the electric permittivity tensor) in a small volume element to be different from that of the surrounding medium. As long as such volume elements are located in the far-field zones of each other, the microphysical approach outlined in section 12 remains applicable, thereby leading to the classical RTE describing multiple Rayleigh scattering [*Chandrasekhar*, 1950]. The specific form of the corresponding extinction and phase matrices

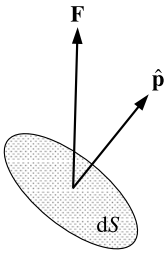

Figure 24. Electromagnetic power through an elementary surface element.

depends on the type of gas (or gas mixture) and on factors such as gaseous pressure and temperature.

[131] It is sometimes stated that the actual cause of Rayleigh scattering are randomly positioned and randomly moving individual molecules rather than electric permittivity fluctuations. However, molecules can often be separated by distances much smaller than the wavelength, thereby grossly violating the far-field zone assumption used to derive the RTE. Of course, one cannot exclude completely the possibility that the RTE can be derived without the far-field zone assumption, but until and unless this is done, it is more prudent to attribute Rayleigh scattering to molecular fluctuations rather than to the individual molecules.

[132] Quite often a gaseous medium contains randomly distributed macroscopic particles. Typical examples are aerosols and cloud particles suspended in a planetary atmosphere. The RTE still remains applicable provided that the particles and the density/anisotropy fluctuations are located in the far-field zones of each other. The phase and extinction matrices entering the RTE are obtained by straightforward averaging over the gas-particle mixture.

17. ENERGY CONSERVATION

[133] An interesting and practically important property of the RTE is that it satisfies precisely the energy conservation law. Indeed, using the vector identity $\mathbf{a} \cdot \nabla f = \nabla \cdot (\mathbf{a}f) - f\nabla \cdot \mathbf{a}$, where f is any scalar function of spatial coordinates, and taking into account that $\hat{\mathbf{q}}$ is a constant vector, we can rewrite equation (60) in the form

$$\nabla \cdot \left[\hat{\mathbf{q}}\, \tilde{\mathbf{I}}(\mathbf{r}, \hat{\mathbf{q}})\right] = -n_0 \langle \mathbf{K}(\mathbf{r}, \hat{\mathbf{q}}) \rangle_\xi \tilde{\mathbf{I}}(\mathbf{r}, \hat{\mathbf{q}}) + n_0 \int_{4\pi} d\hat{\mathbf{q}}' \langle \mathbf{Z}(\hat{\mathbf{q}}, \hat{\mathbf{q}}') \rangle_\xi \tilde{\mathbf{I}}(\mathbf{r}, \hat{\mathbf{q}}'). \quad (67)$$

Let us now introduce the flux density vector as

$$\mathbf{F}(\mathbf{r}) = \int_{4\pi} d\hat{\mathbf{q}} \hat{\mathbf{q}} \tilde{I}(\mathbf{r}, \hat{\mathbf{q}}). \quad (68)$$

Obviously, the product $\hat{\mathbf{p}} \cdot \mathbf{F}(\mathbf{r}) dS$ gives the amount and the direction of the net flow of power through a surface element dS normal to $\hat{\mathbf{p}}$ (see Figure 24). Integrating both sides of equation (67) over all directions $\hat{\mathbf{q}}$ yields [*Mishchenko et al.*, 2006a]

$$-\nabla \cdot \mathbf{F}(\mathbf{r}) = n_0 \int_{4\pi} d\hat{\mathbf{q}} \langle C_{\rm abs}(\hat{\mathbf{q}}) \rangle_\xi \tilde{I}(\mathbf{r}, \mathbf{q}), \quad (69)$$

where $\langle C_{\rm abs}(\hat{\mathbf{q}}) \rangle_\xi$ is the ensemble-averaged absorption cross section per particle. The physical meaning of this formula is very transparent: the net inflow of electromagnetic power per unit volume is equal to the total power absorbed per unit volume. If the particles forming the scattering medium are nonabsorbing so that $\langle C_{\rm abs}(\hat{\mathbf{q}}) \rangle_\xi = 0$, then the flux density vector is divergence-free:

$$\nabla \cdot \mathbf{F}(\mathbf{r}) = 0. \quad (70)$$

This is a manifestation of the conservation of the power flux, which means that the amount of electromagnetic energy entering a volume element per unit time is equal to the amount of electromagnetic energy leaving the volume element per unit time.

[134] The discussion in section 12 clearly shows that the RTE follows from the Maxwell equations only after several simplifying assumptions have been made. Therefore, the fact that the RTE fully complies with the energy conservation law is as much troubling as it is encouraging. Indeed, attempting to improve the accuracy of RTE predictions by including the maximally crossed diagrams appears to destroy energy conservation by adding the ''surplus'' energy contained in the CB intensity peak. It remains unclear whether this additional energy is ''taken'' from the far wings of the backscattering peak, which would imply that the contribution of the maximally crossed diagrams to the specific intensity at certain reflection directions may be negative [cf. *van Tiggelen et al.*, 1995]. It is also possible that the negative contribution restoring energy conservation is supplied by all the other diagram types not accounted for by the microphysical RT and WL theories.

18. DISCUSSION

[135] The discussion in sections 12 and 13 shows that the theories of RT and WL follow from the macroscopic frequency domain Maxwell equations as a consequence of several well-defined approximations. This does not mean, of course, that all of these approximations are mandatory and that the RT and WL theories cannot be derived under less restrictive assumptions. However, until and unless the latter has been done, it is prudent to consider the approximations introduced in sections 12 and 13 as necessary.

[136] An instructive way to look at the microphysical approach to RT and WL is in terms of the famous classification of the methods used to solve problems of wave propagation in random media into two categories, called ''honest'' and ''dishonest'' [*Keller*, 1962]. Specifically, let us assume that a wave is described by a vector-valued function $\mathbf{u}(\mathbf{r}, t)$ of the position vector and time. As in section

10, we denote by ψ the full set of parameters defining the state of the entire scattering medium at a moment in time. According to *Keller* [1962, p. 228],

> in an honest method the solution $\mathbf{u}(\mathbf{r}, t, \psi)$ is first determined for each value of ψ. The solution may sometimes be found exactly and explicitly, but more often it is expressed in the form of a series in some parameter, or as a sequence of iterates, or by some other approximation procedure. In the process of solving for $\mathbf{u}(\mathbf{r}, t, \psi)$ randomness plays no role, and therefore it provides no advantage. The second step is to compute the mean value of $\mathbf{u}(\mathbf{r}, t, \psi)$, as well as its variance and other statistics, from the explicit expression. In this step randomness may have the helpful effect of yielding simpler expressions for the statistics of $\mathbf{u}$ than those for $\mathbf{u}$ itself. In a dishonest method randomness is utilized before $\mathbf{u}(\mathbf{r}, t, \psi)$ is determined. In all cases probability is introduced before $\mathbf{u}$ is determined and an unproved assumption is made about some statistical property of the random wave motion. The assumption usually simplifies the problem so that it becomes solvable.

The reader can easily recognize that the microphysical approach to RT and WL described above belongs to the category of ''honest'' methods.

[137] Figure 25 provides a schematic summary of the microphysical theories of RT and WL and classifies their place within the broader context of classical macroscopic electromagnetics. It also helps to formulate problems that still await solution.

[138] First of all, by using as the starting point the macroscopic frequency domain Maxwell equations, we have completely excluded from consideration such phenomena as emission and frequency redistribution as well as situations involving finite beam and/or pulsed illumination. These areas of electromagnetic energy transfer remain purely phenomenological (e.g., *Ivanov* [1969], *Oxenius* [1986], *Hanel et al.* [2003], *Mätzler* [2006], *Wehrse and Kalkofen* [2006], *Ito et al.* [2007], and references therein) and invoke the RTE without strict derivation from first physical principles. As usual, the use of ''photons'' is widespread, but the electromagnetic field is rarely, if ever, quantized explicitly.

[139] Another challenging area of research is RT in stochastic heterogeneous media composed of widely separated yet spatially correlated particles. For example, it has been suggested in recent publications [*Shaw et al.*, 2002; *Knyazikhin et al.*, 2005a; *Marshak et al.*, 2005] that cloud droplets belonging to a particular size range may tend to form groups of spatially correlated particles (clusters) imbedded in an otherwise homogeneous cloud. It was shown by *Mishchenko* [2006] on the basis of the microphysical approach that as long as such inclusions are small and specific assumptions of ergodicity and spatial uniformity hold, one can still apply the classical RTE in which the participating extinction and phase matrices are obtained by averaging the respective single-particle matrices over all the particles constituting the cloud. However, this result may not necessarily apply to clouds with larger inhomogeneities.

[140] Apart from *Mishchenko* [2006], the problem of multiple scattering in stochastic media composed of widely separated yet correlated particles has been analyzed so far by using the motley concepts of the phenomenological RT theory, including the fictitious ''photons'' (e.g., *Pomraning* [1991], *Cairns et al.* [2000], *Kostinski* [2001], *Petty* [2002], *Barker et al.* [2003], *Borovoi* [2006], *Davis* [2006], and references therein). We have seen in section 12 that the extinction and phase matrices appear in the standard RTE as a consequence of well-defined assumptions and approximations and only as ensemble-averaged quantities. In the phenomenological stochastic RT theory, the extinction and phase matrices are taken for granted and are postulated to be the primary optical attributes of the individual particles. In this sense the phenomenological theory belongs to the category of ''dishonest'' methods. Clearly, a systematic application of the ''honest'' microphysical approach is necessary to determine whether and to what extent the concepts of extinction and phase matrices can be applied to correlated particles.

[141] Many geophysical scattering media are composed of densely packed and strongly correlated particles. Typical examples are snow [*Wiscombe and Warren*, 1980; *Dozier and Painter*, 2004; *Kaasalainen et al.*, 2006], soil [*Irons et al.*, 1992], and regolith surfaces [*Hapke*, 1993; *Shkuratov et al.*, 2007] as well as vegetation [*Myneni et al.*, 1992]. There is a rapidly growing number of publications in which numerical solutions of the RTE are used to model directional reflectance and transmittance characteristics of the various densely packed particulate media (see, e.g., *Leroux et al.* [1999], *Mishchenko et al.* [1999], *Petrova et al.* [2001], *Kokhanovsky* [2004], *Liang* [2004], *Okin and Painter* [2004], *Knyazikhin et al.* [2005b], *Tanikawa et al.* [2006], *Xie et al.* [2006], and references therein). The reader can recall that the formal applicability of the RT theory rests on the assumption that scattering particles are located in each other's far-field zones and are uncorrelated. The obvious violation of these assumptions in the case of densely packed particles can lead to significant deviations from the numerical predictions based on the RTE. Therefore, it is important to analyze both theoretically and experimentally to what extent the classical RT theory can be applied to densely packed particulate media. Some progress in this direction has been reported by *Sergent et al.* [1998], *Hespel et al.* [2003], *Painter and Dozier* [2004], *Pitman et al.* [2005], and *Zhang and Voss* [2005].

[142] The rigorous analytical theory of electromagnetic energy transport in densely packed particulate media is still at an early stage of development [*Tsang and Kong*, 2001; *Tsang et al.*, 2007; *Tishkovets*, 2007]. There are several ''dishonest'' phenomenological approaches to this problem that start with the notion of ''independent scattering'' and attempt to predict the modification of the phase and extinction matrices by effects of packing density, but the heuristic value of such approximations is limited, and their range of validity is unknown [*Hapke*, 1993]. The same is true of the phenomenological approaches based on the use of the geometric optics approximation and Monte Carlo ray tracing, even if electric fields rather than Stokes column vectors are traced [e.g., *Stankevich et al.*, 2007]. Fortu-

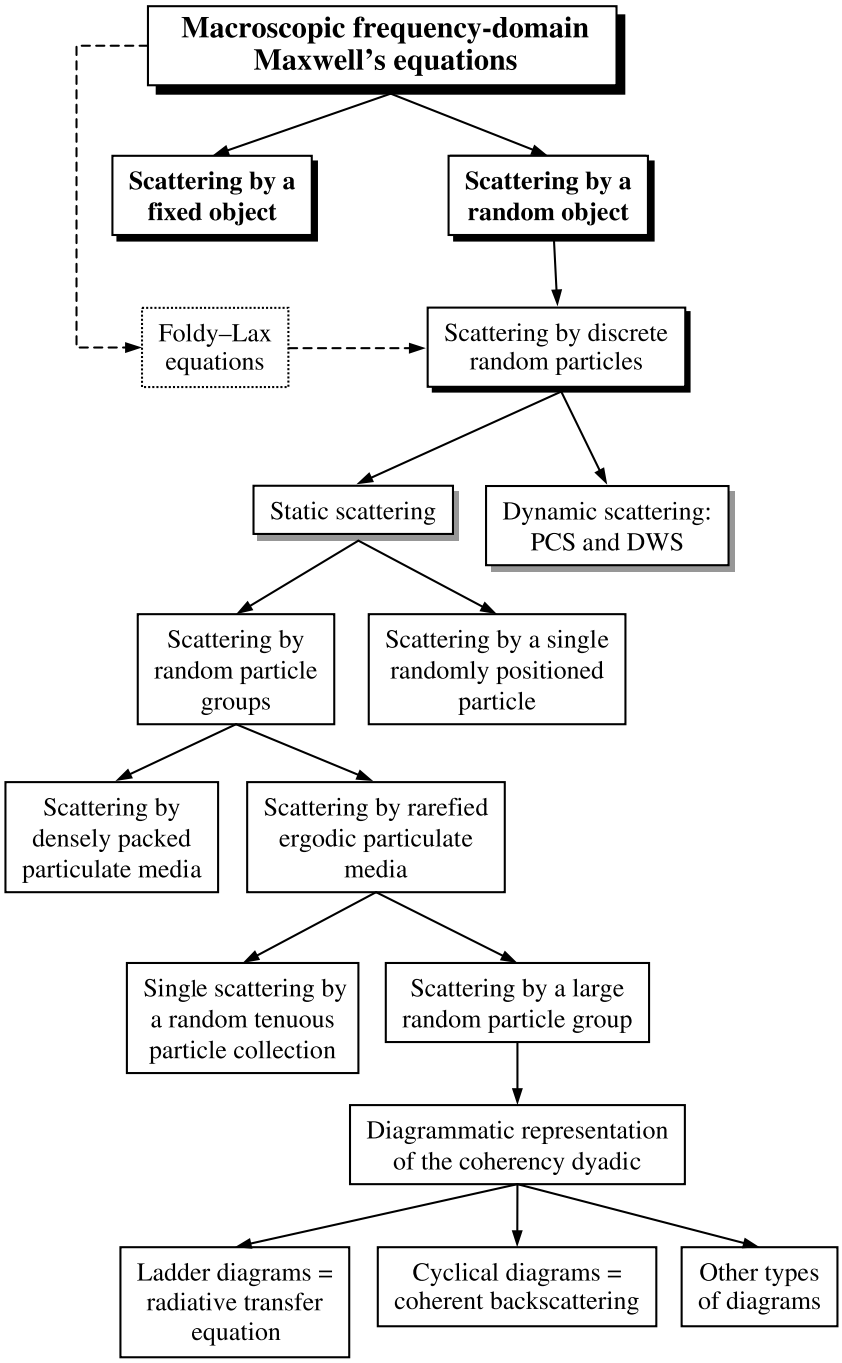

Figure 25. Classification of electromagnetic scattering problems.

nately, as we have seen in section 11, the ever increasing power of scientific workstations and the availability of efficient numerical techniques have led to the emergence of an accurate quantitative approach to this complex problem based on direct computer solutions of the Maxwell equations [*Mackowski*, 2006; *Tseng et al.*, 2006; *Mishchenko and Liu*, 2007; *Mishchenko et al.*, 2007a].

[143] Another important problem is electromagnetic scattering by a medium composed of randomly positioned particles and adjacent to a random rough boundary such as the ocean surface. Although problems like this one are important in practice and have been treated using various phenomenological approaches, microphysical treatments based on consistent application of the Maxwell equations have been extremely scarce.

19. SUMMARY

[144] If one can address the problem of electromagnetic scattering by a volume of discrete random medium using a numerically exact solver of the Maxwell equations, then the final result is accurate for any directions of incidence and

scattering and fully complies with energy conservation. There is no need to invoke the mathematical concept or multiple scattering, to subdivide the exact solution into artificial parts such as the forward scattering interference component, the RT component, the CB component, etc., and to distinguish artificially between ''independent-scattering'' and ''dependent-scattering'' regimes. Therefore, direct numerical solvers of the Maxwell equations should be used as much as possible both to predict the radiative properties of a discrete random medium and as an integral part of noninvasive particle characterization techniques.

[145] For practical reasons, the range of applicability of the above direct approach is still quite limited, thereby justifying the use of an approximate methodology. Still, one should always ensure that the approximate computational technique can be traced directly to a fundamental physical theory and is self-consistent. Hence the great heuristic value of the unified microphysical approach outlined in this review. Indeed, the microphysical approach has demonstrated that the theories of RT and WL are closely related and are, in fact, approximate solutions of the Maxwell equations in that the derivation of neither theory needs any basic physical postulates and concepts other than those contained in classical macroscopic electromagnetics. Furthermore, the origin and exact physical meaning of all participating quantities as well as their relation to more fundamental physical quantities has become clear and unambiguous, while the range of applicability of the theories of RT and WL has become well defined.

[146] Recognizing, understanding, and quantifying the limitations of an approximation is the first step toward a more accurate approach. It is clear in this regard that in order to be physically solvent, any improvement to the RT and WL approximations should originate directly in the Maxwell equations. This is especially true of media composed of densely packed particles. Unfortunately, the rapidly growing complexity of analytical approximations may render them as computer intensive as a numerically exact solution. Therefore, there is little doubt that definitive quantitative analyses of scattering measurements for densely packed particulate media will eventually be based on direct computer solutions of the Maxwell equations. The obvious advantage of this approach is that it can potentially be used to determine all quantitative scattering characteristics of a complex particulate system, including ones that may not be easy to observe.

APPENDIX A: DYADS AND DYADICS

[147] The result of a dyadic operating on a vector is another vector. This operation may be thought of as a 3×3 matrix representing the dyadic multiplying a column matrix consisting of the initial vector components, thereby producing another column matrix consisting of the resulting vector components. The components of both vectors must be specified in the same coordinate system. From a coordinate-free standpoint, a dyadic can be introduced as a sum of so-called dyads, each dyad being the result of a dyadic product of two vectors $\mathbf{a} \otimes \mathbf{b}$ such that the operation $(\mathbf{a} \otimes \mathbf{b}) \cdot \mathbf{c}$ yields the vector $\mathbf{a}(\mathbf{b} \cdot \mathbf{c})$ and the operation $\mathbf{c} \cdot (\mathbf{a} \otimes \mathbf{b})$ yields the vector $(\mathbf{c} \cdot \mathbf{a})\mathbf{b}$. Any dyadic can be represented as a sum of at most nine dyads. The vector product $(\mathbf{a} \otimes \mathbf{b}) \times \mathbf{c}$ is defined as a dyad $\mathbf{a} \otimes (\mathbf{b} \times \mathbf{c})$, and $\mathbf{c} \times (\mathbf{a} \otimes \mathbf{b})$ yields $(\mathbf{c} \times \mathbf{a}) \otimes \mathbf{b}$. The dot product of dyads $\mathbf{a} \otimes \mathbf{b}$ and $\mathbf{c} \otimes \mathbf{d}$ yields the dyad $(\mathbf{b} \cdot \mathbf{c})(\mathbf{a} \otimes \mathbf{d})$. For more details see Appendix A of *Mishchenko et al.* [2006a] or Appendix 4 of *Van Bladel* [2007].

[148] **ACKNOWLEDGMENTS.** The author thanks Li Liu for help with *T* matrix computations and Brian Cairns, Jean-Jacques Greffet, Joop Hovenier, Nikolai Khlebtsov, Dan Mackowski, Alexander Marshak, Pinar Mengüç, Victor Tishkovets, Larry Travis, Gorden Videen, Warren Wiscombe, and Ping Yang for numerous illuminating discussions. This research was supported by the NASA Radiation Sciences Program managed by Hal Maring and by the NASA Glory Mission project.

[149] The Editor responsible for this paper was Gerald North. He thanks two anonymous technical reviewers and one anonymous cross-disciplinary reviewer.

REFERENCES

Agarwal, B. M., and M. P. Mengüç (1991), Forward and inverse analysis of single and multiple scattering of collimated radiation in an axisymmetric system, *Int. J. Heat Mass Transfer*, *34*, 633–647.

Akhiezer, A. I., and V. B. Berestetskii (1965), *Quantum Electrodynamics*, John Wiley, New York.

Akhiezer, A. I., and S. V. Peletminskii (1981), *Methods of Statistical Physics*, Pergamon, Oxford, U. K.

Apresyan, L. A., and Y. A. Kravtsov (1996), *Radiation Transfer: Statistical and Wave Aspects*, Gordon and Breach, Basel, Switzerland.

Babenko, V. A., L. G. Astafyeva, and V. N. Kuzmin (2003), *Electromagnetic Scattering in Disperse Media: Inhomogeneous and Anisotropic Particles*, Springer, Berlin.

Barabanenkov, Y. N. (1975), Multiple scattering of waves by ensembles of particles and the theory of radiation transport, *Sov. Phys. Usp., Engl. Trans.*, *18*, 673–689.

Barabanenkov, Y. N., Y. A. Kravtsov, V. D. Ozrin, and A. I. Saichev (1991), Enhanced backscattering in optics, *Progr. Opt.*, *29*, 65–197.

Barker, H. W., R. K. Goldstein, and D. E. Stevens (2003), Monte Carlo simulation of solar reflectances for cloudy atmospheres, *J. Atmos. Sci.*, *60*, 1881–1894.

Berne, B. J., and R. Pecora (1976), *Dynamic Light Scattering: With Applications to Chemistry, Biology, and Physics*, John Wiley, New York.

Bohren, C. F., and E. E. Clothiaux (2006), *Fundamentals of Atmospheric Radiation*, Wiley-VCH, Weinheim, Germany.

Boltzmann, L. (1964), *Lectures on Gas Theory*, Univ. of Calif. Press, Berkeley.

Borghese, F., P. Denti, and R. Saija (2007), *Scattering From Model Nonspherical Particles: Theory and Applications to Environmental Physics*, Springer, Berlin.

Borovoi, A. G. (2006), Multiple scattering of short waves by uncorrelated and correlated scatterers, *Light Scattering Rev.*, *1*, 181–252.

Borovoy, A. G. (1966), Method of iterations in multiple scattering: The transfer equation (in Russian), *Izv. Vuzov Fiz.*, 6, 50–54.

Brown, W., (Ed.) (1993), *Dynamic Light Scattering*, Clarendon, Oxford, U. K.

Cairns, B., A. A. Lacis, and B. E. Carlson (2000), Absorption within inhomogeneous clouds and its parameterization in general circulation models, *J. Atmos. Sci.*, *57*, 700–714.

Campbell, B. A. (2002), *Radar Remote Sensing of Planetary Surfaces*, Cambridge Univ. Press, Cambridge, U. K.

Cartigny, J. D., Y. Yamada, and C. L. Tien (1986), Radiative transfer with dependent scattering by particles: part 1—Theoretical investigation, *J. Heat Transfer*, *108*, 608–613.

Chandrasekhar, S. (1950), *Radiative Transfer*, Oxford Univ. Press, Oxford, U. K.

Chandrasekhar, S. (1989), *Radiative Transfer and Negative Ion of Hydrogen*, *Selec. Pap.*, vol. 2, pp. 511–541, Univ. of Chicago Press, Chicago, Ill.

Chwolson, O. (1889), Grundzüge einer mathematischen Theorie der inneren Diffusion des Lichtes, *Bull. Acad. Imp. Sci. St. Petersbourg*, *33*, 221–256.

Colton, D., and R. Kress (1998), *Inverse Acoustic and Electromagnetic Scattering Theory*, Springer, Berlin.

Davis, A. B. (2006), Effective propagation kernels in structured media with broad spatial correlations, illustration with large-scale transport of solar photons through cloudy atmospheres, *Lect. Notes Comput. Sci. Eng.*, *48*, 85–140.

Doicu, A., Y. Eremin, and T. Wriedt (2000), *Acoustic and Electromagnetic Scattering Analysis Using Discrete Sources*, Academic, San Diego, Calif.

Doicu, A., T. Wriedt, and Y. A. Eremin (2006), *Light Scattering by Systems of Particles*, Springer, Berlin.

Dolginov, A. Z., Y. N. Gnedin, and N. A. Silant'ev (1995), *Propagation and Polarization of Radiation in Cosmic Media*, Gordon and Breach, Basel, Switzerland.

Dozier, J., and T. H. Painter (2004), Multispectral and hyperspectral remote sensing of alpine snow properties, *Annu. Rev. Earth Planet. Sci.*, *32*, 465–494.

Fabelinskii, I. L. (1968), *Molecular Scattering of Light*, Plenum, New York.

Farquhar, I. E. (1964), *Ergodic Theory in Statistical Mechanics*, John Wiley, London.

Fearn, H., and W. E. Lamb Jr. (1991), Corrections to the golden rule, *Phys. Rev. A*, *43*, 2124–2128.

French, R. G., A. Verbiscer, H. Salo, C. McGhee, and L. Dones (2007), Saturn's rings at true opposition, *Publ. Astron. Soc. Pac.*, *119*, 623–642.

Fuller, K. A., and D. W. Mackowski (2000), Electromagnetic scattering by compounded spherical particles, in *Light Scattering by Nonspherical Particles: Theory, Measurements, and Applications*, edited by M. I. Mishchenko, J. W. Hovenier, and L. D. Travis, pp. 225–272, Academic, San Diego, Calif.

Fung, A. K. (1994), *Microwave Scattering and Emission Models and Their Applications*, Artech House, Boston, Mass.

Gans, R. (1924), Die Farbe des Meeres, *Ann. Phys.*, *75*, 1–22.

Goody, R. M., and Y. L. Yung (1989), *Atmospheric Radiation: Theoretical Basis*, Oxford Univ. Press, Oxford, U. K.

Gross, P., M. Störzer, S. Fiebig, M. Clausen, G. Maret, and C. M. Aegerter (2007), A precise method to determine the angular distribution of backscattered light to high angles, *Rev. Sci. Instrum.*, *78*, 033105, doi:10.1063/1.2712943.

Hanel, R. A., B. J. Conrath, D. E. Jennings, and R. E. Samuelson (2003), *Exploration of the Solar System by Infrared Remote Sensing*, Cambridge Univ. Press, Cambridge, U. K.

Hansen, J. E., and J. W. Hovenier (1974), Interpretation of the polarization of Venus, *J. Atmos. Sci.*, *31*, 1137–1160.

Hansen, J. E., and L. D. Travis (1974), Light scattering in planetary atmospheres, *Space Sci. Rev.*, *16*, 527–610.

Hapke, B. (1993), *Theory of Reflectance and Emittance Spectroscopy*, Cambridge Univ. Press, Cambridge, U. K.

Harmon, J. K., M. A. Slade, R. A. Vélez, A. Crespo, M. J. Dryer, and J. M. Johnson (1994), Radar mapping of Mercury's polar anomalies, *Nature*, *369*, 213–215.

Heaviside, O. (1950), *Electromagnetic Theory*, Dover, New York.

Hespel, L., S. Mainguy, and J.-J. Greffet (2003), Radiative properties of scattering and absorbing dense media: Theory and experimental study, *J. Quant. Spectrosc. Radiat. Transfer*, *77*, 193–210.

Hovenier, J. W., C. van der Mee, and H. Domke (2004), *Transfer of Polarized Light in Planetary Atmospheres—Basic Concepts and Practical Methods*, Springer, Berlin.

Huffman, D. R. (1988), The applicability of bulk optical constants to small particles, in *Optical Effects Associated With Small Particles*, edited by P. W. Barber and R. K. Chang, pp. 279–324, World Sci., Singapore.

Irons, J. R., G. S. Campbell, J. M. Norman, D. W. Graham, and W. M. Kovalick (1992), Prediction and measurement of soil bidirectional reflectance, *IEEE Trans. Geosci. Remote Sens.*, *30*, 249–260.

Ishimaru, A. (1978), *Wave Propagation and Scattering in Random Media*, Academic, New York.

Ito, S., S. Kobayashi, and T. Oguchi (2007), Multiple-scattering formulation of pulsed beam waves in hydrometeors and its application to millimeter-wave weather radar, *IEEE Geosci. Remote Sens. Lett.*, *4*, 13–17.

Ivanov, V. V. (1969), *Transfer of Radiation in Spectral Lines* (in Russian), Nauka, Moscow. (English translation, Natl. Bur. of Stand., Washington, D. C., 1973.)

Ivanov, V. V. (1994), Making of radiative transfer theory (in Russian), *Tr. Astron. Obs. St. Petersburg Univ.*, *44*, 6–29.

Ivezić, Ž., and M. P. Mengüç (1996), An investigation of dependent/independent scattering regimes using a discrete dipole approximation, *Int. J. Heat Mass Transfer*, *39*, 811–822.

Jackson, J. D. (1999), *Classical Electrodynamics*, John Wiley, New York.

Joosten, J. G. H., E. T. F. Geladé, and P. N. Pusey (1990), Dynamic light scattering by nonergodic media: Brownian particles trapped in polyacrylamide gels, *Phys. Rev. A*, *42*, 2161–2175.

Kaasalainen, S., M. Kaasalainen, T. Mielonen, J. Suomalainen, J. I. Peltoniemi, and J. Näränen (2006), Optical properties of snow in backscatter, *J. Glaciol.*, *52*, 574–584.

Kahnert, F. M. (2003), Numerical methods in electromagnetic scattering theory, *J. Quant. Spectrosc. Radiat. Transfer.*, *79/80*, 775–824.

Keller, J. B. (1962), Wave propagation in random media, *Proc. Symp. Appl. Math.*, *13*, 227–246.

Khlebtsov, N. G., I. L. Maksimova, V. V. Tuchin, and L. V. Wang (2002), Introduction to light scattering by biological objects, in *Handbook of Optical Biomedical Diagnostics*, edited by V. V. Tuchin, pp. 31–167, SPIE Press, Bellingham, Wash.

Kidd, R., J. Ardini, and A. Anton (1989), Evolution of the modern photon, *Am. J. Phys.*, *57*, 27–35.

Knyazikhin, Y., A. Marshak, M. L. Larsen, W. J. Wiscombe, J. V. Martonchik, and R. B. Myneni (2005a), Small-scale drop size variability: Impact on estimation of cloud optical properties, *J. Atmos. Sci.*, *62*, 2555–2567.

Knyazikhin, Y., A. Marshak, and R. B. Myneni (2005b), 3D radiative transfer in vegetation canopies and cloud-vegetation interaction, in *3D Radiative Transfer in Cloudy Atmospheres*, edited by A. Marshak and A. B. Davis, pp. 617–651, Springer, Berlin.

Kobayashi, S., T. Oguchi, S. Tanelli, and E. Im (2007), Backscattering enhancement on spheroid-shaped hydrometeors: Considerations in water and ice particles of uniform size and Marshall-Palmer distributed rains, *Radio Sci.*, *42*, RS2001, doi:10.1029/2006RS003503.

Kokhanovsky, A. A. (2004), *Light Scattering Media Optics: Problems and Solutions*, Praxis, Chichester, U. K.

Kostinski, A. B. (2001), On the extinction of radiation by a homogeneous but spatially correlated random medium, *J. Opt. Soc. Am. A Opt. Image Sci.*, *18*, 1929–1933.

Kumar, S., and C. L. Tien (1990), Dependent absorption and extinction of radiation by small particles, *J. Heat Transfer*, *112*, 178–185.

Kuz'min, V. L., and V. P. Romanov (1996), Coherent phenomena in light scattering from disordered systems, *Phys. Usp.*, *39*, 231–260.

Kuz'min, V. L., V. P. Romanov, and L. A. Zubkov (1994), Propagation and scattering of light in fluctuating media, *Phys. Rep.*, *248*, 71–368.

Labeyrie, G., C. A. Müller, D. S. Wiersma, C. Miniatura, and R. Kaiser (2000), Observation of coherent backscattering of light by cold atoms, *J. Opt. B Quantum Semiclassical Opt.*, *2*, 672–685.

Lamb, W. E., Jr. (1995), Anti-photon, *Appl. Phys. B*, *60*, 77–84.
Lenke, R., and G. Maret (2000), Multiple scattering of light: Coherent backscattering and transmission, in *Scattering in Polymeric and Colloidal Systems*, edited by W. Brown, and K. Mortensen, pp. 1–73, Gordon and Breach, Amsterdam, Netherlands.
Lenoble, J. (Ed.) (1985), *Radiative Transfer in Scattering and Absorbing Atmospheres: Standard Computational Procedures*, A. Deepak, Hampton, Va.
Lenoble, J. (1993), *Atmospheric Radiative Transfer*, A. Deepak, Hampton, Va.
Leroux, C., J. Lenoble, G. Brogniez, J. W. Hovenier, and J. F. de Haan (1999), A model for the bidirectional polarized reflectance of snow, *J. Quant. Spectrosc. Radiat. Transfer*, *61*, 273–285.
Liang, S. (2004), *Quantitative Remote Sensing of Land Surfaces*, John Wiley, Hoboken, N. J.
Liou, K. N. (1992), *Radiation and Cloud Processes in the Atmosphere: Theory, Observation, and Modeling*, Oxford Univ. Press, New York.
Liou, K. N. (2002), *An Introduction to Atmospheric Radiation*, Academic, San Diego, Calif.
Lommel, E. (1887), Die Photometrie der diffusen Zurückwerfung, *Sitzber. Acad. Wissensch. München*, *17*, 95–124.
Mackowski, D. W. (2006), Direct simulation of scattering and absorption by particle deposits, paper presented at Proceedings of International Mechanical Engineering Congress and Exposition, Am. Soc. of Mech. Eng., Chicago, Ill.
Mackowski, D. W., and M. I. Mishchenko (1996), Calculation of the *T* matrix and the scattering matrix for ensembles of spheres, *J. Opt. Soc. Am. A Opt. Image Sci.*, *13*, 2266–2278.
Mandel, L., and E. Wolf (1995), *Optical Coherence and Quantum Optics*, Cambridge Univ. Press, Cambridge, U. K.
Marshak, A., and A. B. Davis (Eds.) (2005), *3D Radiative Transfer in Cloudy Atmospheres*, Springer, Berlin.
Marshak, A., Y. Knyazikhin, M. L. Larsen, and W. J. Wiscombe (2005), Small-scale drop size variability: Empirical models of drop-size-dependent clustering in clouds, *J. Atmos. Sci.*, *62*, 551–558.
Martin, P. A. (2006), *Multiple Scattering: Interaction of Time-Harmonic Waves With N Obstacles*, Cambridge Univ. Press, Cambridge, U. K.
Mätzler, C. (2006), *Thermal Microwave Radiation: Applications for Remote Sensing*, IET Press, London.
Maxwell, J. C. (1879), On Boltzmann's theorem on the average distribution of energy in a system of material points, *Trans. Cambridge Philos. Soc.*, *12*, 547–570.
Meystre, P., and M. Sargent III (1999), *Elements of Quantum Optics*, Springer, Berlin.
Mihalas, D., and B. Weibel-Mihalas (1984), *Foundations of Radiation Hydrodynamics*, Oxford Univ. Press, Oxford, U. K.
Mishchenko, M. I. (1992), Enhanced backscattering of polarized light from discrete random media: Calculations in exactly the backscattering direction, *J. Opt. Soc. Am. A Opt. Image Sci.*, *9*, 978–982.
Mishchenko, M. I. (2002), Vector radiative transfer equation for arbitrarily shaped and arbitrarily oriented particles: A microphysical derivation from statistical electromagnetics, *Appl. Opt.*, *41*, 7114–7134.
Mishchenko, M. I. (2003), Microphysical approach to polarized radiative transfer: Extension to the case of an external observation point, *Appl. Opt.*, *42*, 4963–4967.
Mishchenko, M. I. (2006), Radiative transfer in clouds with small-scale inhomogeneities: The microphysical approach, *Geophys. Res. Lett.*, *33*, L14820, doi:10.1029/2006GL026312.
Mishchenko, M. I., and L. Liu (2007), Weak localization of electromagnetic waves by densely packed many-particle groups: Exact 3D results, *J. Quant. Spectrosc. Radiat. Transfer*, *106*, 616–621.
Mishchenko, M. I., J. M. Dlugach, E. G. Yanovitskij, and N. T. Zakharova (1999), Bidirectional reflectance of flat, optically thick particulate layers: An efficient radiative transfer solution and applications to snow and soil surfaces, *J. Quant. Spectrosc. Radiat. Transfer*, *63*, 409–432.
Mishchenko, M. I., J. W. Hovenier, and L. D. Travis (Eds.) (2000), *Light Scattering by Nonspherical Particles: Theory, Measurements, and Applications*, Academic, San Diego, Calif.
Mishchenko, M. I., L. D. Travis, and A. A. Lacis (2002), *Scattering, Absorption, and Emission of Light by Small Particles*, Cambridge Univ. Press, Cambridge, U. K. (Available at http://www.giss.nasa.gov/~crmim/books.html.)
Mishchenko, M. I., L. D. Travis, and A. A. Lacis (2006a), *Multiple Scattering of Light by Particles: Radiative Transfer and Coherent Backscattering*, Cambridge Univ. Press, Cambridge, U. K.
Mishchenko, M. I., V. K. Rosenbush, and N. N. Kiselev (2006b), Weak localization of electromagnetic waves and opposition phenomena exhibited by high-albedo atmosphereless solar system objects, *Appl. Opt.*, *45*, 4459–4463.
Mishchenko, M. I., L. Liu, D. W. Mackowski, B. Cairns, and G. Videen (2007a), Multiple scattering by random particulate media: Exact 3D results, *Opt. Express*, *15*, 2822–2836.
Mishchenko, M. I., L. Liu, and G. Videen (2007b), Conditions of applicability of the single-scattering approximation, *Opt. Express*, *15*, 7522–7527.
Mobley, C. D. (1994), *Light and Water: Radiative Transfer in Natural Waters*, Academic, San Diego, Calif.
Modest, M. (2003), *Radiative Heat Transfer*, Academic, San Diego, Calif.
Muinonen, K. (2004), Coherent backscattering of light by complex random media of spherical scatterers: Numerical solution, *Waves Random Media*, *14*, 365–388.
Müller, C. (1957), *Foundations of the Mathematical Theory of Electromagnetic Waves* (in German), Springer, Berlin.
Myneni, R. B., G. Asrar, D. Tanré, and B. J. Choudhury (1992), Remote sensing of solar radiation absorbed and reflected by vegetated land surfaces, *IEEE Trans. Geosci. Remote Sens.*, *30*, 302–314.
Newton, R. G. (1982), *Scattering Theory of Waves and Particles*, Springer, New York.
Nisato, G., P. Hébraud, J.-P. Munch, and S. J. Candau (2000), Diffusing-wave-spectroscopy investigation of latex particle motion in polymer gels, *Phys. Rev. E*, *61*, 2879–2887.
Okin, G. S., and T. H. Painter (2004), Effect of grain size on remotely sensed spectral reflectance of sandy desert surfaces, *Remote Sens. Environ.*, *89*, 272–280.
Ostro, S. J. (1993), Planetary radar astronomy, *Rev. Mod. Phys.*, *65*, 1235–1279.
Oxenius, J. (1986), *Kinetic Theory of Particles and Photons*, Springer, Berlin.
Painter, T. H., and J. Dozier (2004), Measurements of the hemispherical-directional reflectance of snow at fine spectral and angular resolution, *J. Geophys. Res.*, *109*, D18115, doi:10.1029/2003JD004458.
Petrova, E. V., W. J. Markiewicz, and H. U. Keller (2001), Regolith surface reflectance: A new attempt to model, *Solar Syst. Res.*, *35*, 278–290.
Petty, G. W. (2002), Area-average solar radiative transfer in three-dimensionally inhomogeneous clouds: The independently scattering cloudlet model, *J. Atmos. Sci.*, *59*, 2910–2929.
Pike, R., and P. Sabatier, (Eds.) (2001), *Scattering: Scattering and Inverse Scattering in Pure and Applied Science*, 2 vols., Academic, San Diego, Calif.
Pitman, K. M., M. J. Wolff, and G. C. Clayton (2005), Application of modern radiative transfer tools to model laboratory quartz emissivity, *J. Geophys. Res.*, *110*, E08003, doi:10.1029/2005JE002428.
Poincaré, H. (1890), Sur le problème des trois corps et les équations de la Dynamique, *Acta Math.*, *13*, 1–270.
Pomraning, G. C. (1973), *The Equations of Radiation Hydrodynamics*, Pergamon, Oxford, U. K.
Pomraning, G. C. (1991), *Linear Kinetic Theory and Particle Transport in Stochastic Mixtures*, World Sci., Singapore.

Power, E. A. (1964), *Introductory Quantum Electrodynamics*, Longmans, London.
Preisendorfer, R. W. (1965), *Radiative Transfer on Discrete Spaces*, Pergamon, Oxford, U. K.
Psarev, V., A. Ovcharenko, Y. Shkuratov, I. Belskaya, and G. Videen (2007), Photometry of particulate surfaces at extremely small phase angles, *J. Quant. Spectrosc. Radiat. Transfer*, *106*, 455–463.
Pusey, P. N., and W. van Megen (1989), Dynamic light scattering by non-ergodic media, *Phys. A*, *157*, 705–741.
Rosenbush, V., N. Kiselev, V. Avramchuk, and M. Mishchenko (2002), Photometric and polarimetric opposition phenomena exhibited by solar system bodies, in *Optics of Cosmic Dust*, edited by G. Videen and M. Kocifaj, pp. 191–224, Kluwer, Dordrecht, Netherlands.
Rothwell, E. J., and M. J. Cloud (2001), *Electromagnetics*, CRC Press, Boca Raton, Fla.
Rozenberg, G. V. (1955), Stokes vector-parameter (in Russian), *Usp. Fiz. Nauk*, *56*(1), 77–110.
Saxon, D. S. (1955), Lectures on the scattering of light, *Sci. Rep. 9*, Dep. of Meteorol., Univ. of Calif., Los Angeles, Los Angeles.
Scheffold, F., S. E. Skipetrov, S. Romer, and P. Schurtenberger (2001), Diffusing-wave spectroscopy of nonergodic media, *Phys. Rev. E*, *63*, 061404, doi:10.1103/PhysRevE.63.061404.
Schiff, L. I. (1968), *Quantum Mechanics*, McGraw-Hill, New York.
Schuster, A. (1905), Radiation through a foggy atmosphere, *Astrophys. J.*, *21*, 1–22.
Sergent, C., C. Leroux, E. Pougatch, and F. Guirado (1998), Hemispherical-directional reflectance measurements of natural snow in the 0.9–1.45 μm spectral range: Comparison with adding-doubling modeling, *Ann. Glaciol.*, *26*, 59–63.
Shaw, R. A., A. B. Kostinski, and M. L. Larsen (2002), Towards quantifying droplet clustering in clouds, *Q. J. R. Meteorol. Soc.*, *128*, 1043–1057.
Sheng, P. (2006), *Introduction to Wave Scattering, Localization, and Mesoscopic Phenomena*, Springer, Berlin.
Shkuratov, Y., S. Bondarenko, V. Kaydash, G. Videen, O. Muñoz, and H. Volten (2007), Photometry and polarimetry of particulate surfaces and aerosol particles over a wide range of phase angles, *J. Quant. Spectrosc. Radiat. Transfer*, *106*, 487–508.
Siegel, R., and J. R. Howell (2002), *Thermal Radiation Heat Transfer*, Taylor and Francis, New York.
Silver, S. (1949), Radiation from current distributions, in *Microwave Antenna Theory and Design*, edited by S. Silver, pp. 61–106, McGraw-Hill, New York.
Sobolev, V. V. (1975), *Light Scattering in Planetary Atmospheres*, Pergamon, Oxford, U. K.
Stankevich, D., L. Istomina, Y. Shkuratov, and G. Videen (2007), The scattering matrix of random media consisting of large opaque spheres calculated using ray tracing and accounting for coherent backscattering enhancement, *J. Quant. Spectrosc. Radiat. Transfer*, *106*, 509–519.
Stephens, G. L. (1994), *Remote Sensing of the Lower Atmosphere*, Oxford Univ. Press, New York.
Stokes, G. G. (1852), On the composition and resolution of streams of polarized light from different sources, *Trans. Cambridge Philos. Soc.*, *9*, 399–416.
Stratton, J. A. (1941), *Electromagnetic Theory*, McGraw-Hill, New York.
Taflove, A., and S. C. Hagness (2000), *Computational Electrodynamics: The Finite-Difference Time-Domain Method*, Artech House, Boston, Mass.
Tanikawa, T., T. Aoki, M. Hori, A. Hachikubo, O. Abe, and M. Aniya (2006), Monte Carlo simulations of spectral albedo for artificial snowpacks composed of spherical and nonspherical particles, *Appl. Opt.*, *45*, 5310–5319.
Thomas, G. E., and K. Stamnes (1999), *Radiative Transfer in the Atmosphere and Ocean*, Cambridge Univ. Press, Cambridge, U. K.
Tien, C. L. (1988), Thermal radiation in packed and fluidized beds, *J. Heat Transfer*, *110*, 1230–1242.
Tishkovets, V. P. (2007), Incoherent and coherent backscattering of light by a layer of densely packed random medium, *J. Quant. Spectrosc. Radiat. Transfer*, *108*, 454–463.
Townes, C. H. (1984), Ideas and stumbling blocks in quantum electronics, *IEEE J. Quantum Electron.*, *20*, 547–550.
Tsang, L., and J. A. Kong (2001), *Scattering of Electromagnetic Waves: Advanced Topics*, John Wiley, New York.
Tsang, L., J. A. Kong, and R. T. Shin (1985), *Theory of Microwave Remote Sensing*, John Wiley, New York.
Tsang, L., J. Pan, D. Liang, Z. Li, D. W. Cline, and Y. Tan (2007), Modeling active microwave remote sensing of snow using dense media radiative transfer (DMRT) theory with multiple-scattering effects, *IEEE Trans. Geosci. Remote Sens.*, *45*, 990–1004.
Tseng, S. H., A. Taflove, D. Maitland, and V. Backman (2006), Pseudospectral time domain simulations of multiple light scattering in three-dimensional macroscopic random media, *Radio Sci.*, *41*, RS4009, doi:10.1029/2005RS003408.
Tuchin, V. V., L. V. Wang, and D. A. Zimnyakov (2006), *Optical Polarization in Biomedical Applications*, Springer, Berlin.
Twersky, V. (1964), On propagation in random media of discrete scatterers, *Proc. Symp. Appl. Math.*, *16*, 84–116.
Uhlenbeck, G. E., and G. W. Ford (1963), *Lectures in Statistical Mechanics*, Am. Math. Soc., Providence, R. I.
Ulaby, F. T. and C. Elachi (Eds.) (1990), *Radar Polarimetry for Geoscience Applications*, Artech House, Norwood, Mass.
Van Bladel, J. G. (2007), *Electromagnetic Fields*, IEEE Press, Piscataway, N. J.
van de Hulst, H. C. (1957), *Light Scattering by Small Particles*, John Wiley, New York.
van de Hulst, H. C. (1980), *Multiple Light Scattering*, 2 vols., Academic, New York.
van Rossum, M. C. W., and T. M. Nieuwenhuizen (1999), Multiple scattering of classical waves: Microscopy, mesoscopy, and diffusion, *Rev. Mod. Phys.*, *71*, 313–371.
van Tiggelen, B. A., D. A. Wiersma, and A. Lagendijk (1995), Self-consistent theory for the enhancement factor in coherent backscattering, *Europhys. Lett.*, *30*, 1–6.
Viskanta, R., and M. P. Mengüç (1987), Radiation heat transfer in combustion systems, *Progr. Energy Combust. Sci.*, *13*, 97–160.
von Smoluchowski, M. (1908), Molekular-kinetische Theorie der Opaleszenz von Gasen im kritischen Zustande, sowie einiger verwandter Erscheinungen, *Ann. Phys.*, *25*, 205–226.
Wehrse, R., and W. Kalkofen (2006), Advances in radiative transfer, *Astron. Astrophys. Rev.*, *13*, 3–29.
Wiscombe, W. J., and S. G. Warren (1980), A model for the spectral albedo of snow. I: Pure snow, *J. Atmos. Sci.*, *37*, 2712–2733.
Wolf, E. (1978), Coherence and radiometry, *J. Opt. Soc. Am.*, *68*, 6–17.
Xie, Y., P. Yang, B.-C. Gao, G. W. Kattawar, and M. I. Mishchenko (2006), Effect of ice crystal shape and effective size on snow bidirectional reflectance, *J. Quant. Spectrosc. Radiat. Transfer*, *100*, 457–469.
Xue, J.-Z., D. J. Pine, S. T. Milner, X.-l. Wu, and P. M. Chaikin (1992), Nonergodicity and light scattering from polymer gels, *Phys. Rev. A*, *46*, 6550–6563.
Yanovitskij, E. G. (1997), *Light Scattering in Inhomogeneous Atmospheres*, Springer, Berlin.
Zdunkowski, W., T. Trautmann, and A. Bott (2007), *Radiation in the Atmosphere*, Cambridge Univ. Press, Cambridge, U. K.
Zege, E. P., A. P. Ivanov, and I. L. Katsev (1991), *Image Transfer Through a Scattering Medium*, Springer, Berlin.
Zhang, H., and K. J. Voss (2005), Comparisons of bidirectional reflectance distribution function measurements on prepared particulate surfaces and radiative-transfer models, *Appl. Opt.*, *44*, 597–610.

M. I. Mishchenko, NASA Goddard Institute for Space Studies, 2880 Broadway, New York, NY 10025, USA. (mmishchenko@giss.nasa.gov)